University of Bahrain

College of Science

Department of Physics

Impact of cosmological constraints on inferring the chirp mass of gravitational waves data

By: Raghad Rashed

Student ID: 202011111

Supervised By:

Dr. Walid Azzam

This project report is submitted in partial fulfillment of the requirements for the B.Sc. Degree at the Department of Physics at the

University of Bahrain

First Semester

December 2024

ABSTRACT

The general theory of relativity, proposed in 1915, speculated on the existence of gravitational waves (GWs), where an accelerated mass distorts space, resulting in GWs traveling at the speed of light and carrying information about their progenitors. Over the last few decades, the advanced Laser Interferometer Gravitational-Wave Observatories around the world (LIGO, KAGRA, Virgo), with a sensitivity of measuring the length of the diameter of a proton here use, 10^{-21}m, have succeeded in confirming about 100 detections of gravitational waves (GWs) and studying their compact binary coalescence (CBC) sources. Bayesian statistics is the tool used to decode GW data and estimate the parameters of the GW source, achieved through a computational approach. The GWs have opened many implications and offered a unique tool to reveal cosmology. However, the estimation framework implies uncertainty in measuring the redshift of the GW source. The aim was to apply Hubble parameter H_0 constraints on calculating the chirp mass in the source frame to assess the statistical effect. A Python library was used to estimate the redshift numerically using the luminosity distance and, therefore, to calculate the chirp mass values. The analysis revealed that the high-redshift events lie at a relatively higher standard deviation. We propose that the current GWs observations are not a sensitive tool to probe the cosmological parameters. While increasing the sensitivity of the current ground-based detectors, future observations are more promising to bring insights to cosmology.

Keywords: Gravitational waves (GWs), Compact Binary Coalescence (CBCs), Hubble parameter, Chirp mass, Cosmology.

ACKNOWLEDGMENTS

TABLE OF CONTENTS

LIST OF TABLES

LIST OF FIGURES

LIST OF SYMBOLS

Other symbols

Λ Cosmological constant

$\mathcal{M}$ Chirp mass

μ Friction index

ω Orbital angular frequency

Ω_Λ Cosmological constant density parameter

Ωm Matter density Parameter

d_L Luminosity distance

H_0 Hubble parameter

z Redshift

Physics constants

c Speed of light in a vacuum

G Gravitational constant

Chapter 1

INTRODUCTION

Since telescopes were invented, we've decoded much of the universe's messages through electromagnetic wave observations (X-rays, Gamma rays, Radio waves,...). Leading to amazing discoveries and a torrent of questions. Yet the full cosmic narrative remains untold, with the universe concealing further mysteries. We are currently entering a new era in astronomy, marked by the beginning of multi-messenger observation, following the announcement of the first detection of gravitational waves by the Laser Interferometer Gravitational-Wave Observatory (LIGO) in 2015. Many notable advancements have recently arisen in astrophysics; just last year, in 2023, there was confirmed evidence for detecting stochastic gravitational waves from the very early universe, using nanograph detection techniques. Like, who could have imagined that we could probe the physics at epochs billions of years ago? Or if we would be able to retrieve a "sample" of gravity itself for research? Indeed, this is a groundbreaking discovery, with the next-generation gravitational wave observatories holding exciting potential, and research in gravitational waves is flourishing.Now, we have a new sense of hearing space and a wealth of data to work on!

1

1.1   100 years of hunting the gravity waves

"Mass tells gravity how to curve, and gravity tells mass how to move."

The Newtonian gravity has been the central paradigm of classical physics for centuries and has entirely shaped all that humanity believed about the universe back then. It wasn't until the year 1915, 100 years ago, that a man of physics came up with an idea that was "bizarre": gravity is not a "force"; instead, it is a manifestation of the massive objects present in the fabric of space-time. The time is defined as a extra dimensional in addition to the space dimensions, tracing like a "Fabric". He imagined that an accelerated mass object present in this fabric of space-time would cause a perturbation in this metric, generating a wave that would radiate away from its source at the speed of light, as Einstein's general relativity (GR) proposed **The gravitational waves** (Einstein, 1915). Einstein's theoretical approach to gravitational waves (GWs) cast doubt on their reality; one concern was whether they were a mathematical artifact of Einstein's field equations. If one chose a different coordinate system, they would exceed the speed of light, would no longer be a wave, and would have no physical meaning. Despite that, he couldn't abandon his belief in this phenomenon and deny their existence. After Einstein's death, a debate among scientists arose regarding whether or not GWs transmit energy. This debate was transformed when Richard Feynman attended the conference at Chapel Hill in 1957 and presented his "sticky argument": when a GW propagates transversely on two rings of beads on a bar, the beads will move freely due to the tidal forces, generating friction as a result of heating; thus, GWs must carry energy (DeWitt & Rickles, 2011). The conference inspired the enthusiasm of an engineer, Joseph Weber, who would build his first GWs detector one year later. The idea was to detect the energy released by passing GWs as a sound wave on the bar (Weber, 1960). Weber claimed he detected many of the waves, yet no confirmed detection was announced (Weber, 1971). The GWs remained a mathematical construct; since they are extremely faint and barely interact with matter, detecting them was akin to science fiction or "impossible" for some scientists. In 1974, Joseph Taylor and Russell Hulse announced the first indirect detection of GWs, evidenced by their radiation effects on a binary pulsar system that matched the GR predictions (Taylor et al., 1979), and thus

began the journey of gravitational wave hunting and three decades of development in the science of LIGO.

1.2 The strain

As the GWs pass through space, they "stretch" and "squeeze" the space-time metric itself. The challenge of detecting the GWs was to invent a tool that would measure a quantity change by about 10^{-21}, which is less than the diameter of a proton. This quantity is defined by the "strain," which is a dimensionless quantity relating the change between the detector's two arms L over the length of the arm, given as:

$$h(t) = \frac{\Delta L}{L} \tag{1.1}$$

The gravitational wave signal propagates at the speed of light c as it possesses two polarizations, plus + and cross ×. To make a GW detection, the laser interferometry utilized the enhanced Michelson-Morley interferometry: Two arms are separated by half-beam splitter mirror, where the laser source beam is split into two beams and recombined at the same time and length (Destructive interference). When a gravitational wave pass by the detector, the half "split" laser beams that will recombined and display a slight change in the strain in the photo-detector (Constructive interference), indicating a potential gravitational wave signal detection given as a "Strain Data" (Bailes et al., 2021).
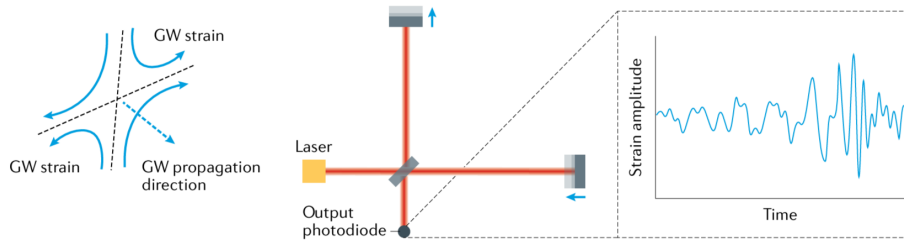
Figure 1.1: *The propagation of a GW,*
   Ligo simple configuration and the Strain amplitude(Bailes et al., 2021).
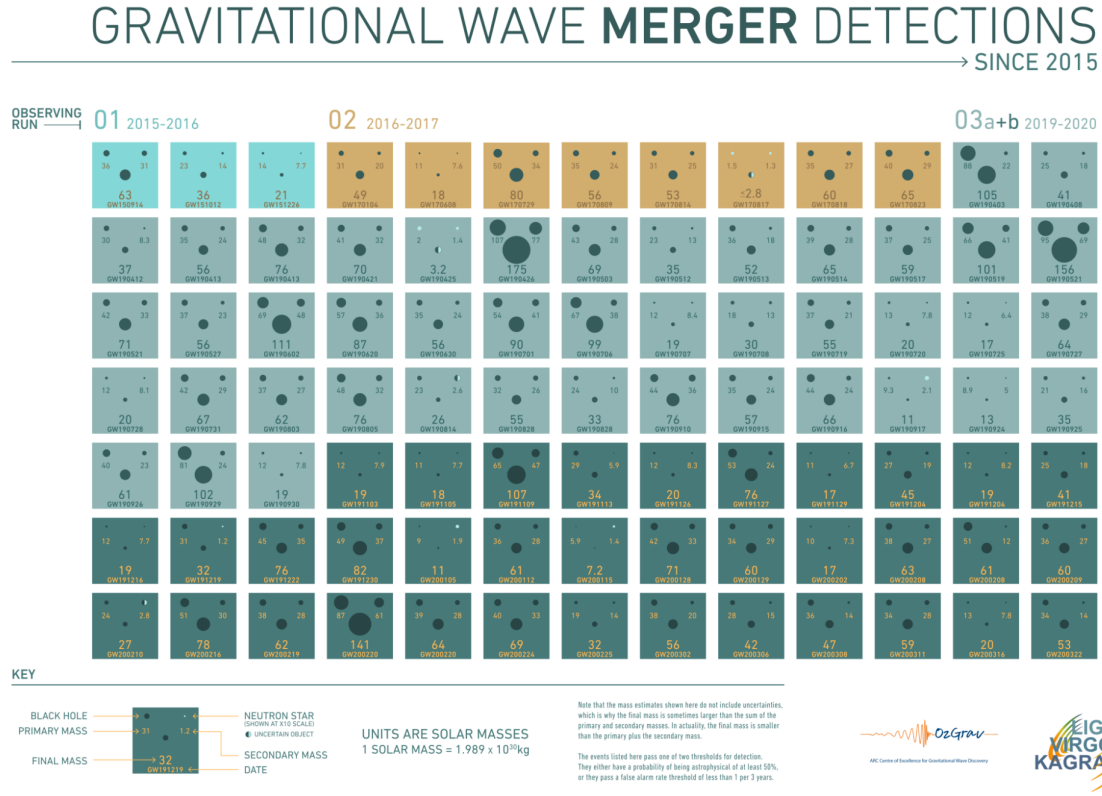
Figure 1.2: The gravitational waves catalog. (R. Abbott, Abe, Acernese, Ackley, et al., 2023)

1.3 Gravitational waves from compact binary coalescence (CBC)

The challenge for the physicist was to make an observational The first detection marked the inception of studying astrophysical objects, GW150914, on 14 September 2015. More than 1.3 billion years ago, two black holes with masses of $23M_\odot$ and $29M_\odot$ solar masses merged into a single black hole, radiating energy in the form of gravitational waves that reached Earth (B. P. Abbott et al., 2016). Since that time, LIGO, in collaboration with a global network of ground-based laser gravitational wave observatories (including the Virgo interferometer in Italy and the KAGRA observatory in Japan), has confirmed more than 100 gravitational wave events in four observation runs (R. Abbott, Abe, Acernese, Ackley, et al., 2023). All the events are attributed to Compact Binary Coalescence (CBC) objects. The compact objects are dense remnants of

	Short Duration	**Long Duration**
Modeled GWs	The CBCs	Continuous waves originated from rotating neutron stars (pulsars). Primordial black holes (PBHs) are believed to have a cosmological origin.
Unmodelled GWs	Burst GWs from supernovae	Stochastic GWs (cosmological origin)

Table 1.1: *Type and sources of gravitational waves*

stars [1]. These objects are found in binary systems where the progenitors can be classified into three categories: 1. Binary Black Holes **(BBH)**, 2. Binary Neutron Stars **(BNS)**, 3. Neutron Star - Black Hole pairs **(NSBH)**. We can classify the gravitational wave sources into two categories: - Inspiral events, in which the binary objects gradually lose energy and spiral closer until they coalesce, - Merger events, where the final coalescence of the binary components results in the emission of gravitational waves and potentially other forms of radiation; refer to Table 1.1. As has been emphasized, the detection of compact binary coalescence (CBCs) has become "routine," whereas no confirmed detection of continuous gravitational waves has yet been established. We expect to achieve this during the upcoming fourth observing run in the next few years, with the enhanced sensitivity of gravitational wave observatories, which will allow for more robust searches for these signals. What do the GWs look like? The frequency band of GWs is broadened in $10^{-18} \lesssim f \lesssim 10^8$, as shown in Figure 1.3. The GWs vary between each source and model; for instance, the chirp waveform of compact binary coalescences (CBCs) differs depending on the characteristics of the binary system, including the masses and spins of the progenitors. However, the overall waveform shares the same phenomenal features[2]. Figure 1.4 illustrates the strain amplitude of the GW150914 signal. In contrast, the "post-merger" is an intrinsic characteristic of the final mass or the "remnant," where the remnant can oscillate and emit GWs as a Ringdown. The neutron star (NS) Ringdown provides information about the

---

[1]Stars spent most of their lives in the main sequences after they eventually collapse and die. Their stellar remanent fate will be either a white dwarfs, black hole or a neutron star, depending on their core mass.

[2]The current Ground-Based detectors can detect the GW signal of the CBC events at their last Inspiral phase, along with the following merger and ring-down phases.
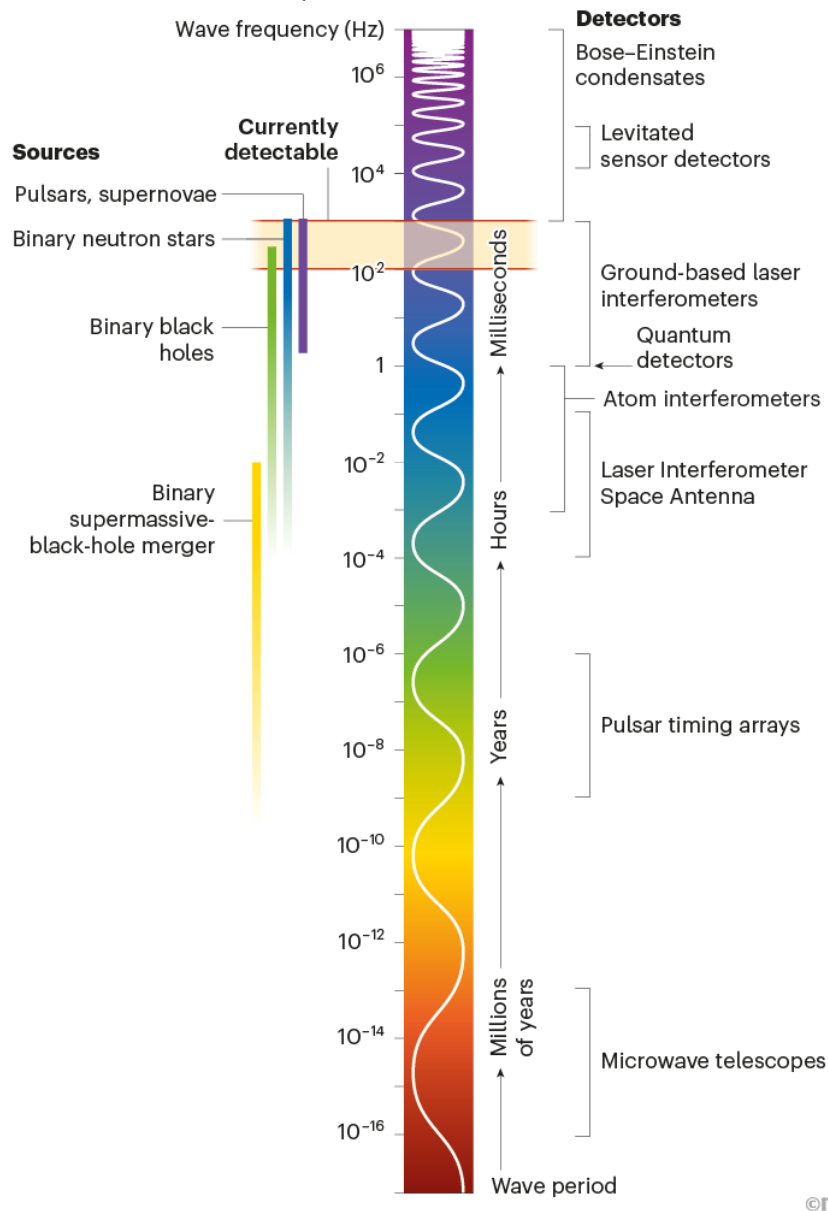
Figure 1.3: Gravitational wave spectrum and the corresponding detectors. The highlighted area is the current state of the GW sensitivity (Bailes et al., 2021).

equation of state (EOS) of nuclear matter, and it typically lasts longer than the ring-down of a black hole remnant (Maione et al., 2017). So, by analyzing the strain data,
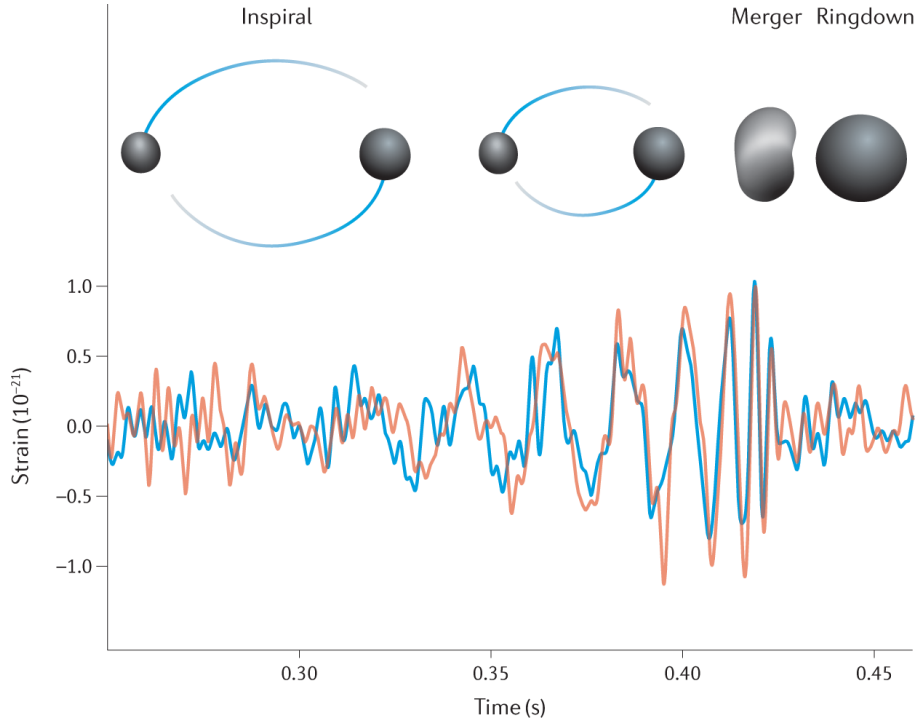
Figure 1.4: *The strain data of GW190814 for the two interferometers (red: Livingston, blue: Hanford). As the orbit of the rotating binary system shrinks (Inspiral phase), the objects get closer, and the frequency and energy increase until they collide (Merging phase). The system forms either a black hole or neutron star final object, releasing energy differences as GWs (Bailes et al., 2021)*

we can study the dynamics of binary systems and infer over 15 parameters, answering questions such as how fast the objects are rotating, how massive they are, and what the merging rate is. Since the dawn of the science of gravitational waves, more than 2000 scientific papers have been published, opening many implications. We can go beyond studying the sources of the signals and even properly assess the **fundamental physics**. That is, we use the generated waveform from the General Relativity (GR) predictions, compare it with our data, and examine how these two have deviated to test various GR parameters (B. Abbott et al., 2019; R. Abbott, Abe, Acernese, Ackley, et al., 2021; R. Abbott, Abbott, Abraham, Acernese, Ackley, Adams, Adams, Adhikari, et al., 2021). The theory passed all the statistical tests by good fortune and seemed fine.

1.3.1   Gravitational waves probing the cosmos

Interestingly, **gravitational wave cosmology** has become a headline lately in GWs science, introducing GWs as a powerful tool that will reach higher redshifts to study various cosmological models, applying constraints on ΛCDM Model and beyond it through the CBCs observations (Z.-C. Chen & Liu, 2024). Two main methods have been proposed to study the cosmology with GWs, The bright siren method: The GW signal can provide a sky localization and a direct measurement of the luminosity distance d_L of their source, If an EM counterpart associated with the detected event signal was observed, the rate at which the universe is expanding can be directly inferred **Hubble constant** H_0 .Using the redshift from the EM data and the luminosity distance of the GWs, We got $H_0 \approx 70$ km/s/Mpc (Mastrogiovanni et al., 2024). Notably, this work suggests a new tool for measuring distance in space with improved accuracy, the "standard siren". If that is not the case and we don't have the EM waves, galaxy catalogs are used to estimate the distances based on the statistical method "Dark siren", leading to a less promising measurement $H_0 \approx 76$ km/s/Mpc (Alfradique et al., 2024).

1.4   Limitation and aim

Gravitational waves are inherently challenging, whether it was experimentally or theoretically. Well, detecting GWs is indeed an arduous procedure. Different types of noise dominate the data, and what we need is to extract a tiny transient signal out of this noisy spectrum and rule out any spurious signal. This process is called match-filtering (Choudhary, 2024), In practice, you are searching for any correlation between the strain data and the template of the CBC waveform. It is not as easy as it sounds; you have a year of running the detectors and a second of passed signal, and you have to do match-filtering for each one, which is necessarily computationally expensive. Machine learning is expected to be involved in solving such problems. After you get the event waveform, you have to infer the parameters of the CBC signal to decide if they are (BBH or BNS, or NSBH). Such a process is called the **parameter estimation**, where you can estimate over 15 parameters for the event (Gair, 2019). Gravitational Wave

Open Science Center (GWOSC) has made great efforts to confirm and study a large portion of such astrophysical events (R. Abbott, Abe, Acernese, Ackley, et al., 2023). However, gravitational wave data alone cannot tell you everything about the event, and you are still searching for the associated EM counterpart for comprehensive observation. Such an event is a blessing; for example, the remarkable event GW170817 of a binary neutron star was associated with detecting a gamma-ray burst (GRB) (B. P. Abbott et al., 2017). That enhanced the sky localization of the source, and astronomers could point their telescopes up there in the sky, resulting in multi-messenger observation (B. P. Abbott, 2017), which led to subsequent studies of the physics and properties of the neutron stars. In the most case scenario, the GW event lacks an EM detection, introduces many limitations lies in using the current GWs data as a tool for probing the cosmos and constraining various cosmological parameters.

In this thesis, a statistical study on the effect of using different Hubble parameters H_0 will be applied to gravitational wave data to examine its effect on the chirp mass under different redshift estimations. In the theory, an overview of GWs parameter estimation and the cosmological model will be provided. In Chapter 4, the results of the analysis of the computed chirp mass and redshift distributions will be discussed, along with the final research status of the events. Finally, a summary and proposed future work will be presented in Chapter 5.

Chapter 2

THEORY

2.1   The parameter estimation

How can we make a statement about the astrophysical object binaries based on the strain data? We use **Bayes theorem**[1]. Based on this theorem, a crucial method for dealing with uncertainty in the GW source parameters is achieved by the **Bayesian statistic**. In practice, the prior knowledge we have about the GWs data is the **prior distribution** $\pi(\theta \mid M)$, which is used to estimate the probability distribution known as the **posterior distribution** $p(\theta \mid d, M)$ via the **evidence** $\mathcal{Z}(d \mid M)$ of the data (Gair, 2019). For model M, let d be the strain data, θ is the set of 15 parameters that we want to estimate. The probability density function of the parameter θ is the posterior distribution, given by Equation (2.1).

$$p(\theta \mid d, M) = \frac{L(d \mid \theta, M)\pi(\theta \mid M)}{\mathcal{Z}(d \mid M)} \tag{2.1}$$

(Gair, 2019).

Here $\mathcal{L}(d|\theta, M)$ is the likelihood function of the data. For the case of the GWs data, the likelihood function is modeled as the Gaussian noise function (the detector noise), which describes the strain measurements for multiple detectors. The posterior evidence [2] defined as

$$\mathcal{Z}(d|M) = \int \mathcal{L}(d|\theta, M)\,\pi(\theta|M)\,d\theta \tag{2.2}$$

---

[1]The GW event is "unique", thus, the estimated parameter of the events is considered to be random variables rather than frequentist (i.e, GW150914 with black holes masses $23M_{\odot}$ and $29M_{\odot}$ is one-of-kind in the universe and all you got is to observe it one time)

[2]The evidence is a normalization factor of the posterior (It's like a single number that can be ignored). However, it acts as a model selection in testing different waveform models/hypotheses.

The posterior and evidence are not known in "closed form" and thus cannot be written down as an analytical solution. The GWOSC research team relies on computational approaches such as "stochastic sampling," usually implemented using Python. It is worth noting that since the posterior results are considered random variables, we can update our posterior distribution by assigning a different prior; hence, we cannot be 100% sure and the choice of the "prior" does affect the updated posterior (Gair, 2019).[3]

2.1.1 The posterior data: Summary statistic

The datasets for gravitational wave parameter estimation are provided as probability distributions. After incorporating prior knowledge, the posterior data is essentially the probability density function (PDF) of a parameter θ that contains the desired "updated" information. To obtain point estimates of a parameter (let's say $\mathcal{M}$), the "marginalized distribution" of the parameter is used:

$$p_{\text{marg}}(\theta_1 \mid \mathbf{x}) = \int p(\vec{\theta} \mid \mathbf{x}) \, d\theta_2 \cdots d\theta_m. \tag{2.3}$$

(Gair, 2019) However, the full posterior cannot be expressed in analytical form. A set of samples N is chosen to compute the integral:

$$\int f(\vec{\theta}) p(\vec{\theta} \mid \mathbf{x}) \, d\vec{\theta} \approx \frac{1}{N} \sum_{i=1}^{N} f(\vec{\theta}_i). \tag{2.4}$$

The **mean**, for example, can also be computed (e.g., the chirp mass $\mathcal{M}$):

$$\mu = \frac{1}{N} \sum_{i=1}^{N} \mathcal{M}_i \tag{2.5}$$

Where $\{\theta_i\}$ are the datasets of the posterior samples (e.g., the chirp mass datasets for each time measurement t).

---

[3]The event GW230529, announced in May 2023, has a secondary mass object that falls within the mass gap, which remains ambiguous. Using a different prior, different posterior beliefs about the progenitors are introduced (Chattopadhyay et al., 2024)

2.1.2 Kernel Density Estimation

Now, for non-parametric distributions, such as redshift (z), kernel density estimation (KDE) is generally used to estimate the posterior probability density function (PDF). For $\{\theta_i\}$ posterior data (Here is the redshift z), KDE is defined as:

$$\hat{f}(z) = \frac{1}{Nh} \sum_{i=1}^{n} K\left(\frac{z - z_i}{h}\right),$$

(2.6)

where K is the kernel function (e.g., Gaussian), h is the bandwidth parameter, and N is the sample size of the dataset, (Gair, 2019).

2.1.3 Credible Interval

A credible interval is a span within which the "true value" of a parameter is found with a given probability. For a parameter θ, the credible interval $[a, b]$ indicates:

$$\int_{a}^{b} P(\theta \mid \mathcal{D}) d\theta = \alpha$$

(2.7)

where α represents the desired credibility level (e.g., $\alpha = 0.90$ for 90% credible interval). The 90% credible interval is derived from the posterior samples and represents the range within which the parameter lies with 90% probability (Gair, 2019). This approach ensures accurate representation and visualization of posterior data. This study used Python as a reliable tool.

2.2 The chirp mass

As previously established in the Introduction, the gravitational waveform signals generated by compact binary coalescence (CBC) events follow a characteristic pattern roughly described by three main cycles (Inspiral, Merging, and Ring-down).
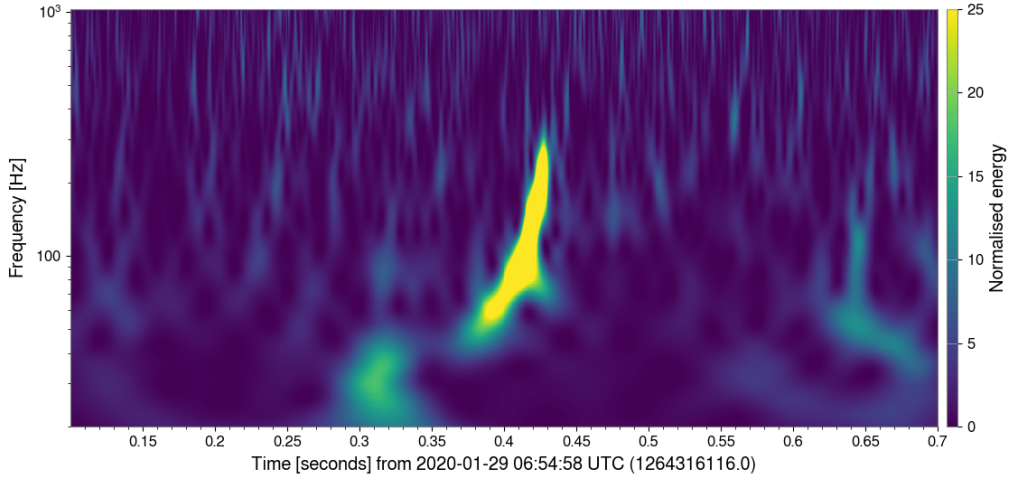
Figure 2.1: *The Time-frequency domain of the strain data of the gravitational wave event GW200129_065458, with two massive black holes of primary mass 34.5M_⊙ and secondary 29.0M_⊙*

The binary system evolves during the in-spiral phase[4], and its orbital frequency increases, causing the system to emit higher-frequency gravitational waves. The energy loss due to radiated GW energy will cause the orbital frequency to "shrink" until the objects merge. In Figure 2.1, a rapid increase in the strain amplitude, a "boost" for the event, is evident from the color-map scale around the time 0.4 seconds. This marks the point at which we introduce a key parameter of the gravitational wave strain-data: the **chirp mass** $\mathcal{M}$.

To elucidate further, let's proceed with an example of two point-like black holes orbiting each other with masses of m_1 and m_2, at position vectors $\mathbf{r_1}$ and $\mathbf{r_2}$. In the Newtonian framework, the system dynamics can be described as a one-body problem orbiting around the center of mass **CM**. The masses are reduced to what we call the reduced mass $\mu = \frac{m_1 m_2}{m_1 + m_2}$. The solution to Newton's equation is just Kepler's Third law, where the orbital angular frequency is

$$\omega^2 = \frac{GM}{r^3} \tag{2.8}$$

---

[4]The In-spiral phase of a compact binary coalescence (CBC) can span for hundreds of million years after its formation. In the case of NS-NS binary pulsar system, the coalescence time is 2786 Myr!
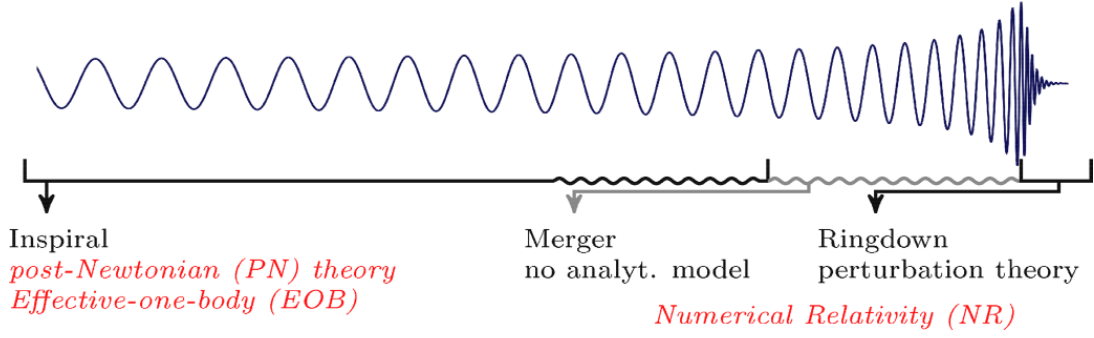
Figure 2.2: *During the very last In-spirel phase, the orbital properties of the system decays as the Keplerian model can't be applicable and numerical relativity is needed.As this dynamics change occurs at very slow process, the Post-Newtonian physics can still provide a good approximation(Ohme, 2011).*

Here, M is the total mass, then $M = m_1 + m_2$ and r is the relative coordinate $r = \mathbf{r_2} - \mathbf{r_1}$, which can be written as:

$$\vec{r_1} = \frac{m_2\vec{r}}{m_1 + m_2}, \quad \vec{r_2} = -\frac{m_1\vec{r}}{m_1 + m_2} \tag{2.9}$$

By expressing r in favor of ω, we introduce the chirp mass quantity $\mathcal{M} = \eta^{\frac{3}{5}}M^{\frac{2}{5}}$, usually described as(Scientific & Collaborations, 2017):

$$\mathcal{M} = \frac{(m_1 m_2)^{3/5}}{(m_1 + m_2)^{1/5}} \tag{2.10}$$

The "mass ratio" is expressed as (Scientific & Collaborations, 2017):

$$q = \frac{m_2}{m_1} \tag{2.11}$$

The chirp mass is the binary system's fingerprint on the strain data, a quantity that can be directly inferred (using Bayesian statistics) from the **detector** frame. Importantly, this approach is valid under the assumption of "circular orbits" in the binary system(Scientific & Collaborations, 2017). For equal-mass binaries, the rest-frame argument holds, and hence the Keplerian regime can be applied. For more compact systems (i.e., unequal-mass binaries) the gravitational potential is large, and the arguments used above can be less effective; such complexity requires numerical relativity, see Figure 2.2.

2.3   Cosmology model

Notice that the quantities we have introduced so far are given in the detector frame. However, for gravitational wave signals propagating at a higher stage (i.e., compact binary coalescence (CBC) objects occurring at high redshift 0.25-1 on the Gpc scale), these observations should be affected by the cosmological redshift.Now, how can we obtain the actual "source frame" estimated quantities? Reminding you of **The Friedmann–Robertson–Walker metric (FRW)**: The universe is "isotropic and homogeneous" [5], the "metric" is the main quantity that can describe the geometry of the universe on the Gpc scale (Husa, 2009):

$$ds^2 = -c^2 dt^2 + a^2(t)\left[\frac{dr^2}{1-kr^2} + r^2\left(d\theta^2 + \sin^2\theta\, d\phi^2\right)\right] \tag{2.12}$$

where: $a(t)$ is the **scale factor** of the universe, t is the cosmic time, r,θ,ϕ are the comoving coordinates, k is the curvature parameter (k=0 for a flat universe, k=+1 for a closed universe, k=-1 for gravitational waves (GWs) propagate through space-time at the speed of light (c). For a GW propagating radially, the angular component term in 2.12 can be ignored, applying the condition $ds^2 = 0$. Substituting this into the FRW metric (Husa, 2009):

$$0 = -c^2 dt^2 + a^2(t)\frac{dr^2}{1-kr^2}. \tag{2.13}$$

To make things easier, a flat universe is assumed $k = 0$, leading to:

$$c\, dt = a(t)\, dr. \tag{2.14}$$

Thus, the comoving distance r covered by a GW is related to the time evolution of the scale factor $a(t)$.(Husa, 2009)

---

[5]Homogeneous means that the universe structure is uniformly distributed everywhere. Isotropic means that the universe looks the same in all directions, without a preferred direction.

2.3.1 Emission and Observation Times

Consider a "binary system" at comoving distance r emitting two successive GW wave polarizations at times t_{source} and $t_{\text{source}} + \Delta t_{\text{source}}$. These wavefronts are detected at the observer's location at times t_{obs} and $t_{\text{obs}} + \Delta t_{\text{obs}}$.

Using the metric condition (2.14), the propagation of GWs gives:

$$\int_{t_{\text{source}}}^{t_{\text{obs}}} \frac{c\,dt}{a(t)} = \int_0^r dr. \tag{2.15}$$

Since the comoving distance r is fixed for the source, the same equation applies to both wavefronts. Subtracting the two propagation equations for successive wavefronts:

$$\int_{t_{\text{source}}}^{t_{\text{source}}+\Delta t_{\text{source}}} \frac{c\,dt}{a(t)} = \int_{t_{\text{obs}}}^{t_{\text{obs}}+\Delta t_{\text{obs}}} \frac{c\,dt}{a(t)}. \tag{2.16}$$

The scale factor $a(t)$ can be approximated as constant during each interval, hence (Husa, 2009):

$$\frac{\Delta t_{\text{source}}}{a(t_{\text{source}})} = \frac{\Delta t_{\text{obs}}}{a(t_{\text{obs}})}. \tag{2.17}$$

The **redshift** z of the source is defined as:

$$1 + z = \frac{a(t_{\text{obs}})}{a(t_{\text{source}})}. \tag{2.18}$$

Thus, the relationship between the time intervals becomes:

$$\Delta t_{\text{obs}} = (1 + z)\,\Delta t_{\text{source}}. \tag{2.19}$$

The frequency of a GW is just $f = 1/\Delta t$. The derived relationship 2.19 implies:

$$f_{\text{obs}} = \frac{1}{\Delta t_{\text{obs}}} = \frac{1}{(1+z)\,\Delta t_{\text{source}}} = \frac{f_{\text{source}}}{1+z} \tag{2.20}$$

This framework analysis shows that the observed frequency is redshifted by the factor $1 + z$ (Husa, 2009).

2.3.2   Luminosity Distance and chirp mass source frame

The above analysis suggests that for CBCs at a cosmological distance, the frequency of the GW source is not the value measured in the detector frame. By the same token, the **chirp mass** $\mathcal{M}$, which determines the frequency evolution of the waveform, is also redshifted(Maggiore, 2018). The observed chirp mass $\mathcal{M}_{\text{obs}}$ is related to the source-frame chirp mass $\mathcal{M}_{\text{source}}$ as:

$$\mathcal{M}_{\text{obs}} = (1 + z)\mathcal{M}_{\text{source}}. \tag{2.21}$$

The amplitude of the GW signal depends on the luminosity distance D_L, which is related to the redshift as (Maggiore, 2018):

$$D_L = (1 + z)a(t_0)r,$$

where $a(t_0)$ is the present-day scale factor, and r is the comoving distance. (Maggiore, 2018)

2.4   Cosmological constrains on inferring the gravitational waves parameters.

2.4.1   The redshift

In the previous section, we proved that gravitational wave signals are affected by redshift, similar to electromagnetic waves. However, gravitational wave signals are inherently "opaque"; we cannot directly measure the redshift as we do with electromagnetic signals. In fact, it is rare to detect an associated electromagnetic counterpart with a

gravitational wave (GW) event; such an event is remarkable [6]. In this context, we estimate the luminosity distance as a function of redshift. For each H_0, the luminosity distance D_L is related to z via (Mastrogiovanni et al., 2024):

$$D_L = \frac{c}{H_0} \int_0^z \frac{dz'}{\sqrt{\Omega_m(1+z')^3 + \Omega_\Lambda}}. \tag{2.22}$$

If you have the GWs luminosity distance D_L directly inferred from the signal strain data, and you define the cosmological parameters:Ω_m (Matter Density Parameter)[7] and Ω_Λ (Cosmological Constant Parameter)[8], the redshift z can be estimated. In this thesis, we will solve the formula **numerically** using Python, as illustrated in 3.2.3 methodology section.

2.4.2 Hubble parameter: Applying a constrain

The Hubble constant, denoted as H_0, represents the current expansion rate of the universe over time. The parameter H_0 plays a vital role in both astrophysical observations and theoretical cosmological models. As in gravitational wave (GW) parameter estimation, the events are "re-weighted" and assigned to a prior in the source comoving frame with an assumed cosmology: The gravitational wave transient catalog analysis assumes a flat ΛCDM cosmology with $H_0 = 67.7\,\mathrm{km\,s^{-1}\,Mpc^{-1}}$, $\Omega_\mathrm{m} = 0.309$ and $\Omega_\Lambda = 1 - \Omega_\mathrm{m}$, consistent with Planck 2018 results (R. Abbott, Abbott, et al., 2023). The masses of gravitational wave events in the source frame are corrected for the source redshift masses, as elucidated in Section 3.2. However, experimental measurements using various methods have introduced a discrepancy between the values of H_0 measured by different experimental techniques. For instance, around 4σ, a discrepancy was reported between the value obtained from the cosmic microwave background (CMB) $H_0 = 67.4 \pm 0.5\,\mathrm{km\ s^{-1}\,Mpc^{-1}}$ and other measurements, like those from

---

[6]GW170817 event had an associated gamma-ray burst detected shortly after 2 minuets by Fermi telescope.

[7]The matter density parameter Ω_m describes the ratio of the matter density to the critical density of the universe.

[8]The cosmological constant parameter Ω_Λ describes the ratio of the energy density of the cosmological constant to the critical density of the universe.

Type Ia supernovae. $H_0 = 73.29 \pm 1.4 \, \text{km s}^{-1} \, \text{Mpc}^{-1}$, (Verde et al., 2023). Such evidence of tension refers to "Hubble tension"; see Figure 2.3 for an example. The statistically significant discrepancy raises concerns about the accuracy of GWs redshift estimates, which represent the methodological issue that will be addressed in the methodology section of this thesis. Three Hubble values will be considered:

- **Cosmic microwave background (CMB)**: $H_0 = 67.4 \, \text{km s}^{-1} \text{Mpc}^{-1}$

- **Time lensing delays**: $H_0 = 74.5 \, \text{km s}^{-1} \, \text{Mpc}^{-1}$

- **Standard Serins**: $H_0 = 70.0 \, \text{km s}^{-1} \, \text{Mpc}^{-1}$
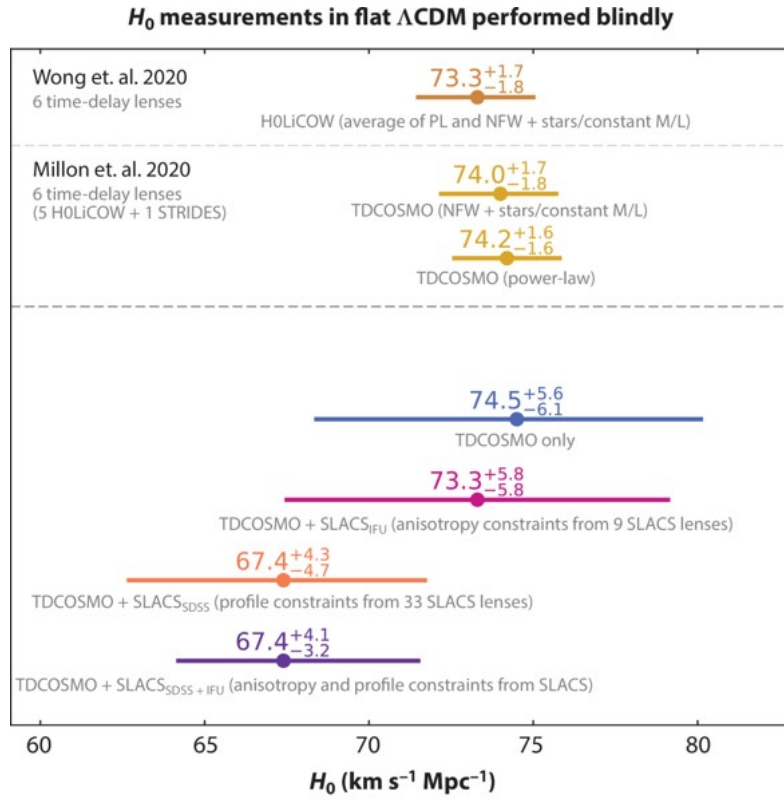
Figure 2.3: *Summary of Hubble constant measurements introduced by the lensing time delays method, an alternative method to estimate Hubble parameter by measuring the relative arrivals time delays of highly gravitational lensed objects (Verde et al., 2023)*

Chapter 3

METHODOLOGY

3.1   Data sampling

The analysis scope spans seven confirmed gravitational wave events from the first, second, and third GW catalogs (B. P. Abbott et al., 2019),(R. Abbott, Abbott, Abraham, Acernese, Ackley, Adams, Adams, Adhikari, et al., 2021),(R. Abbott, Abbott, et al., 2023). The selected events are: GW150914, GW170814, GW190828, GW200112, GW200129, GW200224, and GW200311, with the estimated parameters listed in Table 3.1. All the events are attributed to binary black holes (BBH). For the sake of simplicity, we aimed to choose systems with almost equal masses (i.e., mass ratio in the range $0.8 \leq q \leq 1$), so using the Newtonian mechanism framework described in Section 2.2 is justified, and the relativistic corrections can be ignored. In practice, the event GW200129 is attributed to two massive black holes with a mass ratio of:

$$q = \frac{29}{34.5} = 0.84 \tag{3.1}$$

The event occurs at a distance of 890 Mpc, allowing us to apply statistical analysis where the effect of redshift is relatively significant.

3.2   Framework

A computational approach using **Python** programming language was employed to compute the measurements from the posterior data. The unified code used for all the samples was described by the flowchart configurations, which illustrate the methodological steps 3.1. The rest of the code is listed in Appendix A.
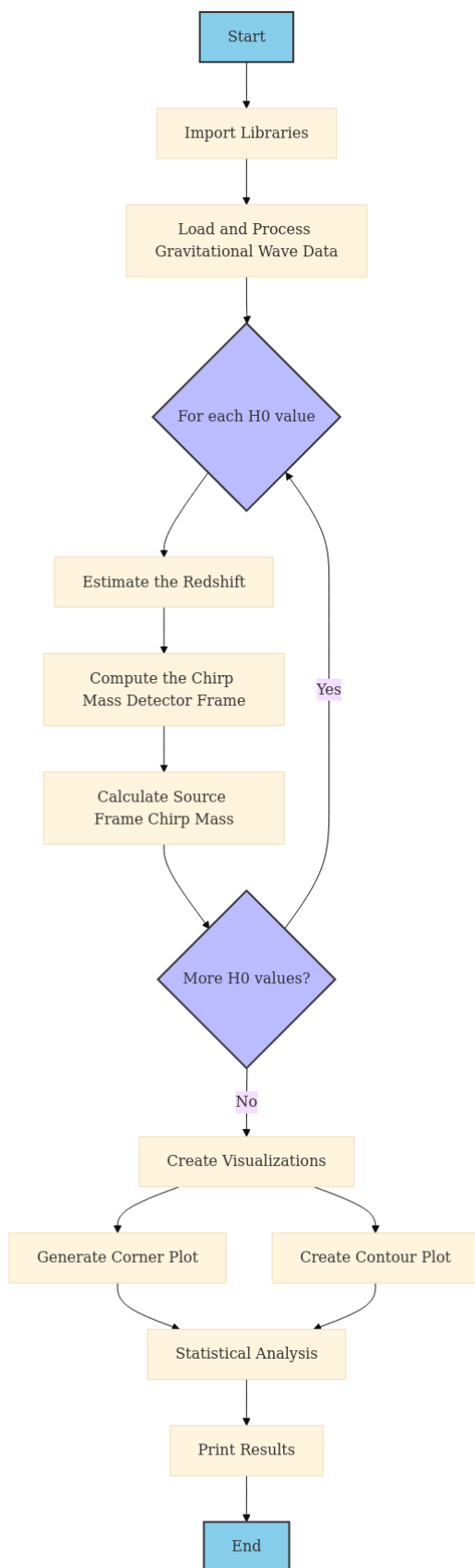
Figure 3.1: *The Python code configuration flowchart*

Event Name	$m_{1,\text{source}}$ ($M_\odot$)	$m_{2,\text{source}}$ ($M_\odot$)	D_L (Gpc)	$\mathcal{M}_{\text{source}}$ ($M_\odot$)	z	E_{GW} ($M_\odot c^2$)	q
GW150914	$35.6^{+4.7}_{-3.1}$	$30.6^{+3.0}_{-4.4}$	$0.44^{+0.15}_{-0.17}$	$28.6^{+1.7}_{-1.5}$	$0.09^{+0.03}_{-0.03}$	$3.1^{+6.53}_{-6.16}$	$0.86^{+4.79}_{-4.63}$
GW170814	$30.6^{+5.6}_{-3.0}$	$25.2^{+2.8}_{-4.0}$	$0.60^{+0.15}_{-0.22}$	$24.1^{+1.4}_{-1.1}$	$0.12^{+0.03}_{-0.04}$	$2.6^{+7.03}_{-5.55}$	$0.82^{+5.16}_{-4.12}$
GW190828_063405	$31.9^{+5.4}_{-4.1}$	$25.8^{+4.9}_{-5.3}$	$2.07^{+0.65}_{-0.92}$	$24.6^{+3.6}_{-2.0}$	$0.38^{+0.10}_{-0.15}$	$2.9^{+10.76}_{-5.87}$	$0.81^{+5.90}_{-5.42}$
GW200112_155838	$35.6^{+6.7}_{-4.5}$	$28.3^{+4.4}_{-5.9}$	$1.25^{+0.43}_{-0.46}$	$27.4^{+2.6}_{-2.1}$	$0.24^{+0.07}_{-0.08}$	$3.1^{+7.78}_{-6.30}$	$0.79^{+6.37}_{-5.90}$
GW200129_065458	$34.5^{+9.9}_{-3.1}$	$29.0^{+3.3}_{-9.3}$	$0.89^{+0.26}_{-0.37}$	$27.2^{+2.1}_{-2.3}$	$0.18^{+0.05}_{-0.07}$	$3.1^{+6.09}_{-4.67}$	$0.84^{+8.77}_{-8.24}$
GW200224_222234	$40.0^{+6.7}_{-4.5}$	$32.7^{+4.8}_{-7.2}$	$1.71^{+0.50}_{-0.65}$	$31.1^{+3.3}_{-2.7}$	$0.32^{+0.08}_{-0.11}$	$3.6^{+9.84}_{-7.15}$	$0.82^{+6.74}_{-6.94}$
GW200311_115853	$34.2^{+6.4}_{-3.8}$	$27.7^{+4.1}_{-5.9}$	$1.17^{+0.28}_{-0.40}$	$26.6^{+2.4}_{-2.0}$	$0.23^{+0.05}_{-0.07}$	$2.9^{+7.15}_{-5.73}$	$0.81^{+6.16}_{-5.68}$

Table 3.1: *The list of the selected gravitational wave events binaries with the corresponding key parameters confirmed by GWOSC.(R. Abbott, Abbott, et al., 2023),(R. Abbott, Abbott, Abraham, Acernese, Ackley, Adams, Adams, Adhikari, et al., 2021),(B. P. Abbott et al., 2019)*

3.2.1 Imported libraries

```python
#For Data processing
import h5py
import bilby
#For creating visuals
import pandas as pd
import matplotlib.pyplot as plt
import numpy as np
from scipy import stats
import seaborn as sns
from matplotlib.colors import Normalize
from matplotlib.cm import ScalarMappable
#To compute the redshift
from astropy.cosmology import z_at_value
from astropy import units as u
from astropy.cosmology import FlatLambdaCDM
```

Code Listing 3.1: *The Python libraries*

3.2.2 Data validation

The posterior samples for all the events were accessed from the public data files provided in the form of HDF5 files, with each event's posterior samples loaded into

GW150914 Chirp Mass Distribution for Different Waveform Models
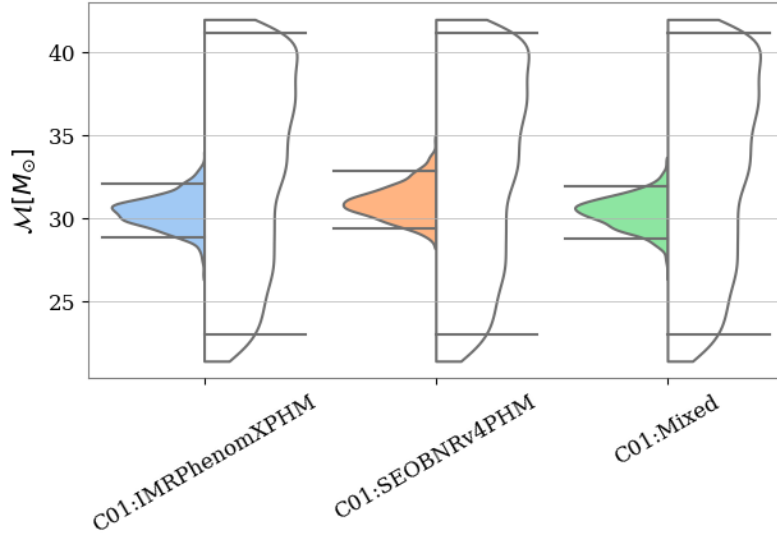
Figure 3.2: *The three different waveforms of the chirp mass posterior data*

Python using the h5py library. The waveform model **"C01:Mixed"** is chosen for all the samples due to its comprehensive posterior parameter distribution, as it effectively combines results from multiple waveform models; see figure 3.2.Posterior samples were transformed into pandas DataFrames for simpler handling.

3.2.3 Main Algorithm

The study assumed the following cosmology: The ΛCDM cosmology model[1] of a flat universe with $k = 0$. The parametrizations are:

- $H_0 = (68.4\,\mathrm{km\,s^{-1}\,Mpc^{-1}}, 70\,\mathrm{km\,s^{-1}\,Mpc^{-1}}, 74.5\,\mathrm{km\,s^{-1}\,Mpc^{-1}})$

- $\Omega_\mathrm{m} = 0.3$

- $\Omega_\Lambda = 1 - \Omega_\mathrm{m} = 0.7$

1. **Redshift Estimation:** By assuming the cosmology, the luminosity distance values from each event posterior samples were used to estimate the redshift posterior for the three H_0 values. This was done using the FlatLambdaCDM cosmology

---

[1]The universe is dominated by a "spatially flat" cosmological constant Λ and the major components of it include (invisible "Dark matter", "baryons" cluster under gravity, and three neutrinos components)

model from the `astropy` library and the `z_at_value` function that numerically estimate the redshift distribution for a given D_L.

2. **Chirp Mass Calculation:** Using the detector-frame masses from the published data of each event, The **detector-frame** chirp mass was estimated using the equation (2.10).

   The **source-frame** chirp mass was then computed by dividing the detector-frame chirp mass by $(1 + z)$ for each redshift value, refer to equation (2.21)

3. **Statistical Analysis:** The mean and standard deviation of the source-frame chirp mass were calculated for each H_0 value. These results were compared to assess the variation in chirp mass due to changes in H_0.

Chapter 4

RESULTS

4.1   Summary statistics

Based on the framework we proposed in the methodology and theory sections, the luminosity distances from the GW data in Table 3.1 were used to estimate the redshift values for each H_0 constraint. From the masses of the seven BBHs listed in 3.1 the chirp mass in the detector frame was computed [1]. The redshifted chirp mass was computed using the relation in formula 2.21 for each estimated redshift value. The summary statistics are provided in the tables listed below for each single GW event, arranged from the oldest (GW150914) to the most recent event (GW200311) in Tables (4.1-4.7).

Refer to the code in the AppendixA, the median was chosen over the mean for the analysis of the posterior distribution. As for the redshift posterior, the distribution is skewed, or "asymmetric". It is non-parametric statistics where the mean value would be affected by the extreme values. However, the mean and median provided in the following tables are almost equal, due to the mass-equal systems of all the chosen signals. In such a case, parameter inference would favor symmetric distributions.

---

[1]In fact, the most reliably constrained parameters we can infer from the GWs data are the masses of the binary system.

(a) Chirp Mass Values (in $M_\odot$)

Parameter	Mean	Median	Std Dev	Lower 90%	Upper 90%
Chirp Mass ($H_0 = 67.4$)	27.9340	27.9210	0.9534	26.4522	29.5568
Chirp Mass ($H_0 = 70.0$)	27.8435	27.8305	0.9503	26.3665	29.4610
Chirp Mass ($H_0 = 74.5$)	27.6890	27.6760	0.9450	26.2201	29.2975
Numerical Relativity	27.9172	27.9172	-	-	-

(b) GW150914 Redshift Values

Parameter	Mean	Median	Std Dev	Lower 90%	Upper 90%
Redshift ($H_0 = 67.4$)	0.0980	0.0991	0.0183	0.0671	0.1257
Redshift ($H_0 = 70.0$)	0.1015	0.1026	0.0189	0.0696	0.1301
Redshift ($H_0 = 74.5$)	0.1076	0.1088	0.0200	0.0739	0.1378
Literature Redshift	0.0987	0.0998	0.0184	0.0676	0.1266

Table 4.1: *Chirp Mass and Redshift summary statistic*

(a) Chirp Mass (in $M_\odot$)

Parameter	Mean	Median	Std Dev	Lower 90%	Upper 90%
Chirp Mass ($H_0 = 67.4$)	24.0640	24.0351	0.7612	22.8817	25.3741
Chirp Mass ($H_0 = 70.0$)	23.9695	23.9406	0.7582	22.7918	25.2744
Chirp Mass ($H_0 = 74.5$)	23.8086	23.7800	0.7531	22.6388	25.1047
Numerical Relativity	24.0714	24.0714	-	-	-

(b) Redshift Values

Parameter	Mean	Median	Std Dev	Lower 90%	Upper 90%
Redshift ($H_0 = 67.4$)	0.1221	0.1246	0.0225	0.0797	0.1544
Redshift ($H_0 = 70.0$)	0.1264	0.1291	0.0232	0.0827	0.1598
Redshift ($H_0 = 74.5$)	0.1339	0.1367	0.0245	0.0877	0.1691
Literature Redshift	0.1230	0.1256	0.0226	0.0803	0.1555

Table 4.2: *GW170814 Chirp Mass and Redshift Values for Different H_0*

(a) Chirp Mass (in $M_\odot$)

Parameter	Mean	Median	Std Dev	Lower 90%	Upper 90%
Chirp Mass ($H_0 = 67.4$)	13.4328	13.4463	0.3115	12.8975	13.9166
Chirp Mass ($H_0 = 70.0$)	13.3328	13.3462	0.3092	12.8015	13.8130
Chirp Mass ($H_0 = 74.5$)	13.1651	13.1783	0.3053	12.6404	13.6392
Numerical Relativity	13.3883	13.3883	-	-	-

(b) Redshift Values

Parameter	Mean	Median	Std Dev	Lower 90%	Upper 90%
Redshift ($H_0 = 67.4$)	0.2875	0.2891	0.0670	0.1786	0.3952
Redshift ($H_0 = 70.0$)	0.2970	0.2988	0.0691	0.1848	0.4081
Redshift ($H_0 = 74.5$)	0.3135	0.3153	0.0726	0.1955	0.4301
Literature Redshift	0.2897	0.2913	0.0676	0.1799	0.3983

Table 4.3: *GW190828_063405 Chirp Mass and Redshift Values for Different H_0*

(a) Chirp Mass (in $M_\odot$)

Parameter	Median	Std Dev	Lower 90%	Upper 90%
Chirp Mass ($H_0 = 67.4$)	27.3604	1.3201	25.4404	29.7204
Chirp Mass ($H_0 = 70.0$)	27.1817	1.3115	25.2742	29.5262
Chirp Mass ($H_0 = 74.5$)	26.8807	1.2970	24.9943	29.1993
Numerical Relativity	27.3956	0	27.3956	27.3956

(b) Redshift Values

Parameter	Median	Std Dev	Lower 90%	Upper 90%
Redshift ($H_0 = 67.4$)	0.2404	0.0464	0.1592	0.3108
Redshift ($H_0 = 70.0$)	0.2486	0.0479	0.1648	0.3211
Redshift ($H_0 = 74.5$)	0.2626	0.0503	0.1743	0.3388
Literature Redshift	0.2422	0.0468	0.1604	0.3132

Table 4.4: *GW200112_155838 Chirp Mass and Redshift Values for Different H_0*

(a) Chirp Mass (in $M_\odot$)

Parameter	Mean	Median	Std Dev	Lower 90%	Upper 90%
Chirp Mass ($H_0 = 67.4$)	27.0693	27.1871	1.1105	24.9511	28.6967
Chirp Mass ($H_0 = 70.0$)	26.9272	27.0443	1.1047	24.8201	28.5460
Chirp Mass ($H_0 = 74.5$)	26.6866	26.8027	1.0948	24.5983	28.2910
Numerical Relativity	27.1588	27.1588	-	-	-

(b) Redshift Values

Parameter	Mean	Median	Std Dev	Lower 90%	Upper 90%
Redshift ($H_0 = 67.4$)	0.1753	0.1794	0.0369	0.1095	0.2295
Redshift ($H_0 = 70.0$)	0.1814	0.1856	0.0381	0.1134	0.2373
Redshift ($H_0 = 74.5$)	0.1918	0.1963	0.0402	0.1202	0.2507
Literature Redshift	0.1766	0.1807	0.0372	0.1103	0.2313

Table 4.5: *GW200129_065458 Chirp Mass and Redshift Values for Different H_0*

(a) Chirp Mass (in $M_\odot$)

Parameter	Mean	Median	Std Dev	Lower 90%	Upper 90%
Chirp Mass ($H_0 = 67.4$)	31.0626	31.1177	1.7351	28.2164	33.7922
Chirp Mass ($H_0 = 70.0$)	30.8176	30.8722	1.7214	27.9938	33.5256
Chirp Mass ($H_0 = 74.5$)	30.4068	30.4606	1.6985	27.6206	33.0787
Numerical Relativity	31.0765	31.0765	-	-	-

(b) Redshift Values

Parameter	Mean	Median	Std Dev	Lower 90%	Upper 90%
Redshift ($H_0 = 67.4$)	0.3092	0.3152	0.0562	0.2079	0.3915
Redshift ($H_0 = 70.0$)	0.3194	0.3257	0.0580	0.2151	0.4042
Redshift ($H_0 = 74.5$)	0.3370	0.3436	0.0609	0.2273	0.4261
Literature Redshift	0.3116	0.3176	0.0567	0.2095	0.3945

Table 4.6: *GW200224_222234 Chirp Mass and Redshift Values for Different H_0*

(a) *Chirp Mass (in $M_\odot$)*

Parameter	Mean	Median	Std Dev	Lower 90%	Upper 90%
Chirp Mass ($H_0 = 67.4$)	26.6013	26.6300	1.3324	24.3859	28.8077
Chirp Mass ($H_0 = 70.0$)	26.4347	26.4633	1.3240	24.2332	28.6273
Chirp Mass ($H_0 = 74.5$)	26.1539	26.1821	1.3100	23.9758	28.3232
Numerical Relativity	26.5966	26.5966	-	-	-

(b) *Redshift Values*

Parameter	Mean	Median	Std Dev	Lower 90%	Upper 90%
Redshift ($H_0 = 67.4$)	0.2228	0.2268	0.0354	0.1564	0.2741
Redshift ($H_0 = 70.0$)	0.2304	0.2345	0.0366	0.1618	0.2833
Redshift ($H_0 = 74.5$)	0.2434	0.2478	0.0385	0.1713	0.2990
Literature Redshift	0.2245	0.2285	0.0357	0.1575	0.2762

Table 4.7: *GW200311_115853 Chirp Mass and Redshift Values for Different H_0*

4.2 Contour Plots

To visualize the posterior data, a corner plot is typically used, which displays the histogram of the distribution along with the density function. Two main plots are shown for the selected events. For instance, in Figure 4.1, the corner plot illustrates the histogram of the three chirp mass values, where the left and right dashed lines highlight the 90% credible regions, representing the 5th and 95th percentiles, respectively. Furthermore, the line fits the "true value" of the given parameter, while the color bar indicates the highest density.

At first glance, you may think that the distributions are equal, but the contour distributions (b) show a clear shift in the least accurate $H_0 = 70$ value, and almost equal values for the more precise Hubble measurements.
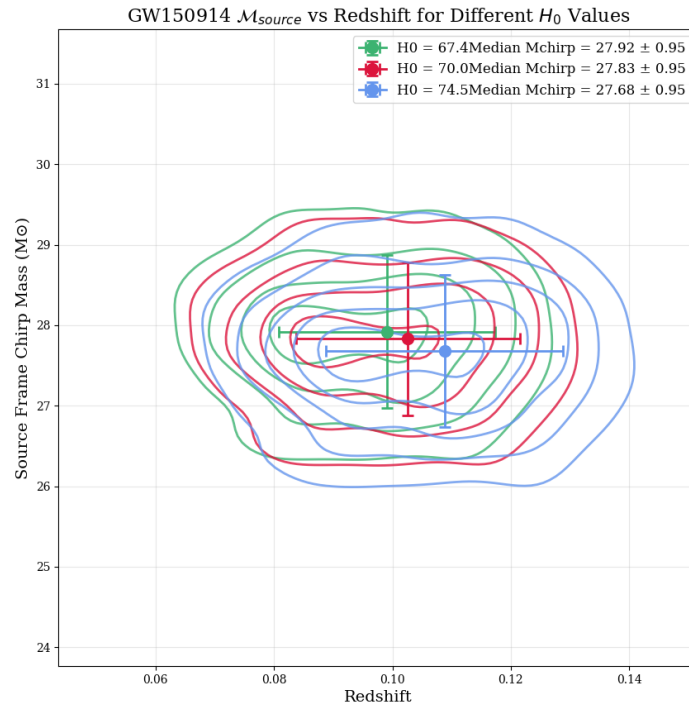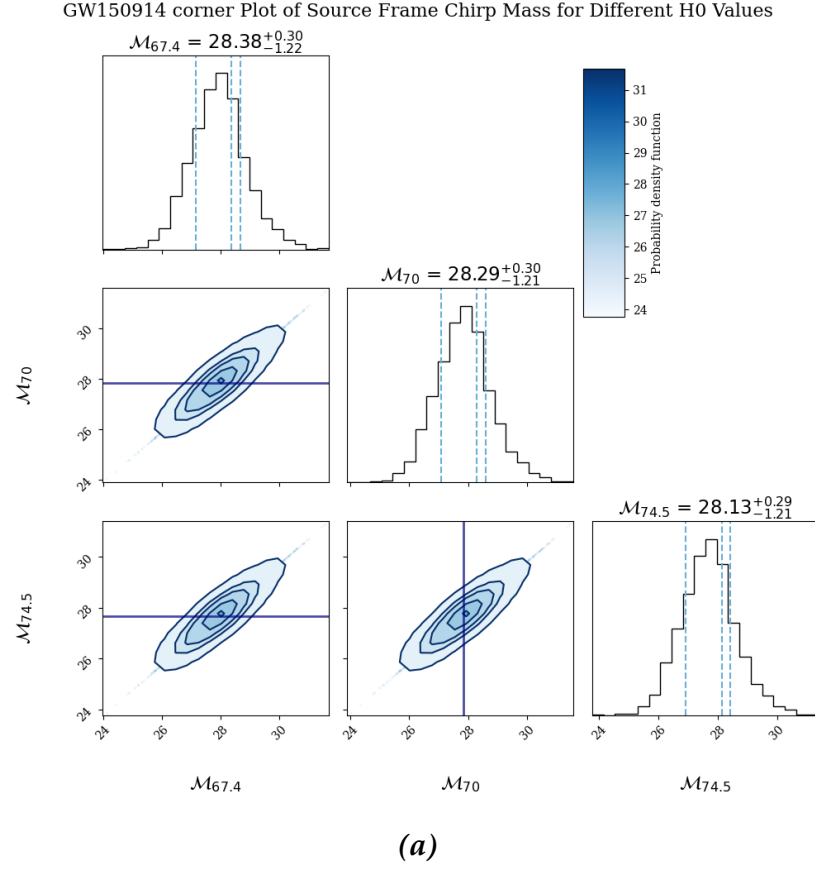
GW150914 corner Plot of Source Frame Chirp Mass for Different H0 Values

(a)

(b)

Figure 4.1: *GW150914: (a) Corner plot for the chirp mass, and (b) contour plot showing the chirp mass as a function of the redshift.*
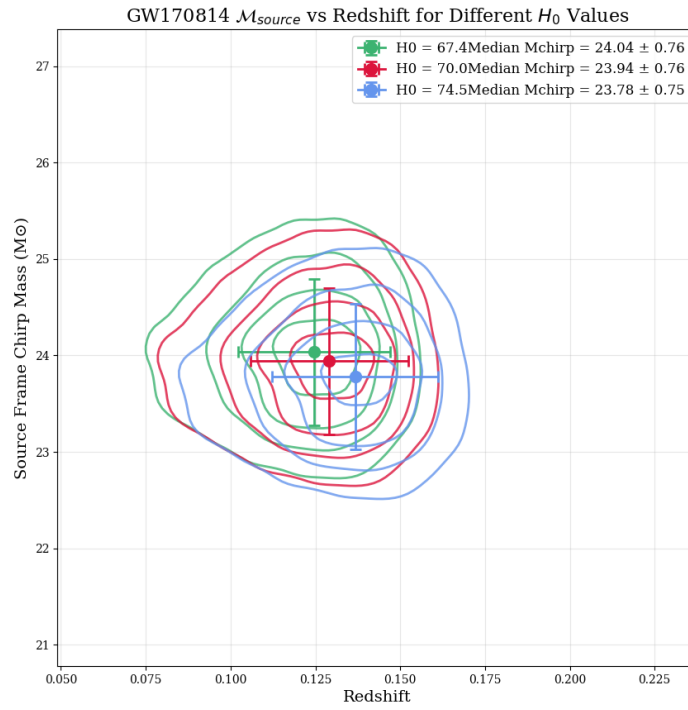
(a)

(b)

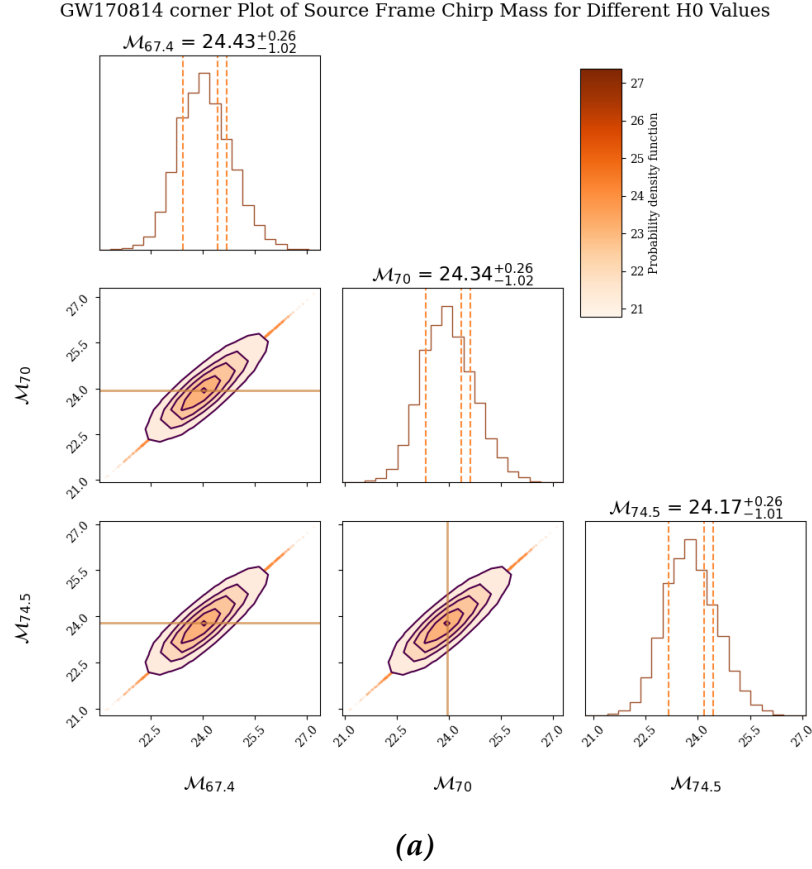**Figure 4.2:** *GW170814: (a) Corner plot for the chirp mass, and (b) contour plot showing the chirp mass as a function of the redshift.*

(a)

(b)

Figure 4.3: *GW190828: (a) Corner plot for the chirp mass, and (b) contour plot showing the chirp mass as a function of the redshift.*

(a)

(b)

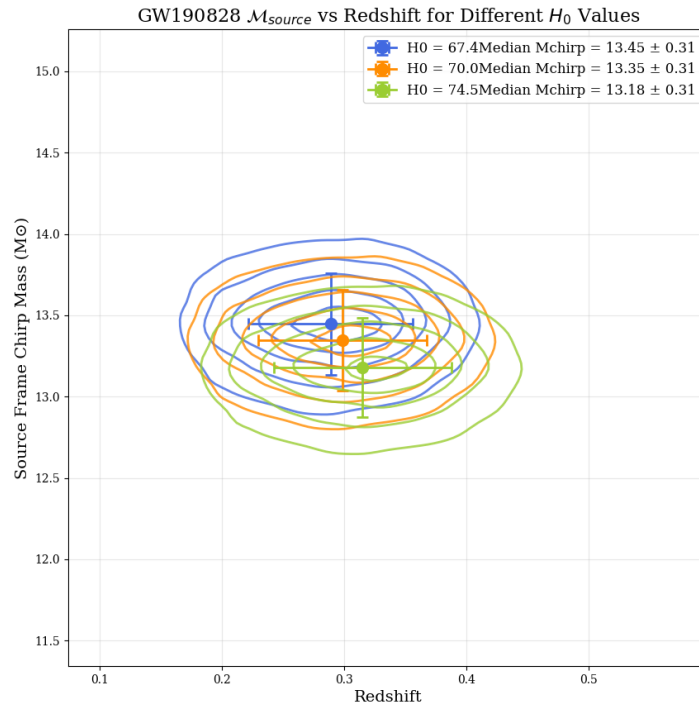**Figure 4.4:** *GW200112: (a) Corner plot for the chirp mass, and (b) contour plot showing the chirp mass as a function of the redshift.*

(a)

(b)

Figure 4.5: *GW200129: (a) Corner plot for the chirp mass, and (b) contour plot showing the chirp mass as a function of the redshift.*

(a)

(b)
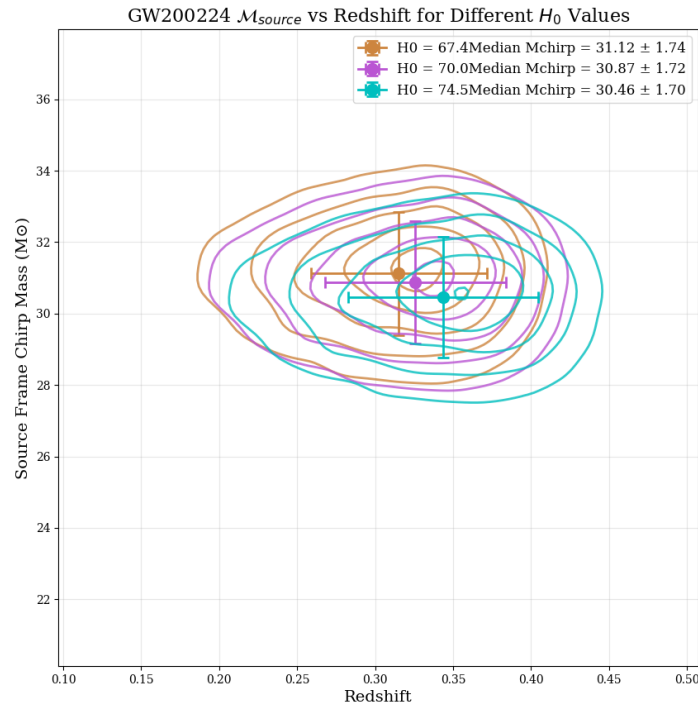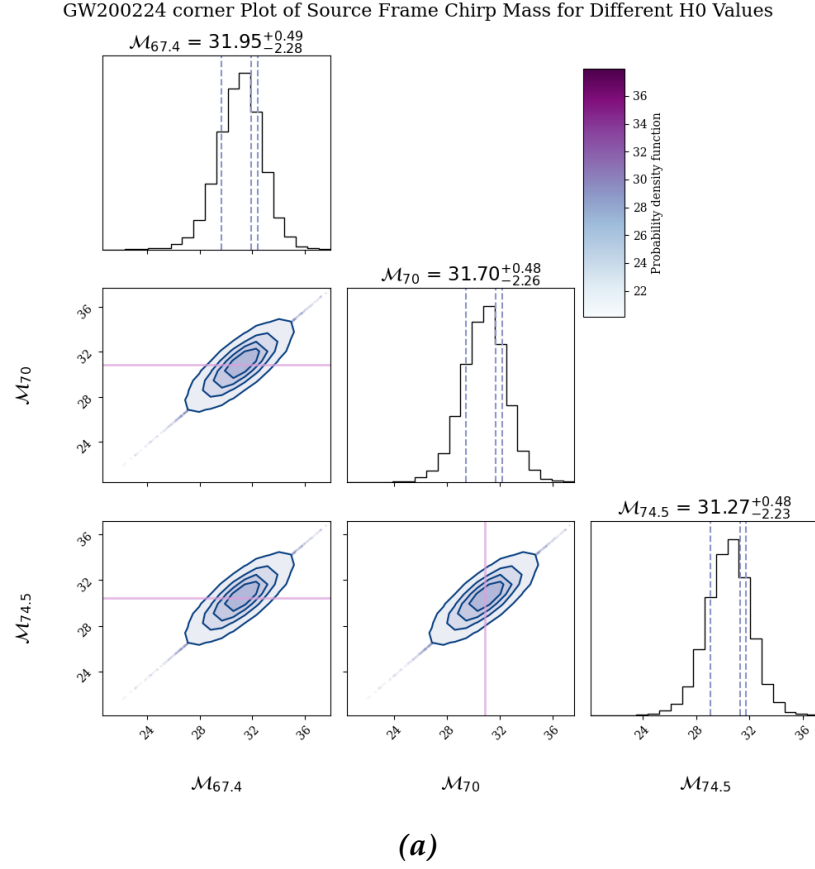
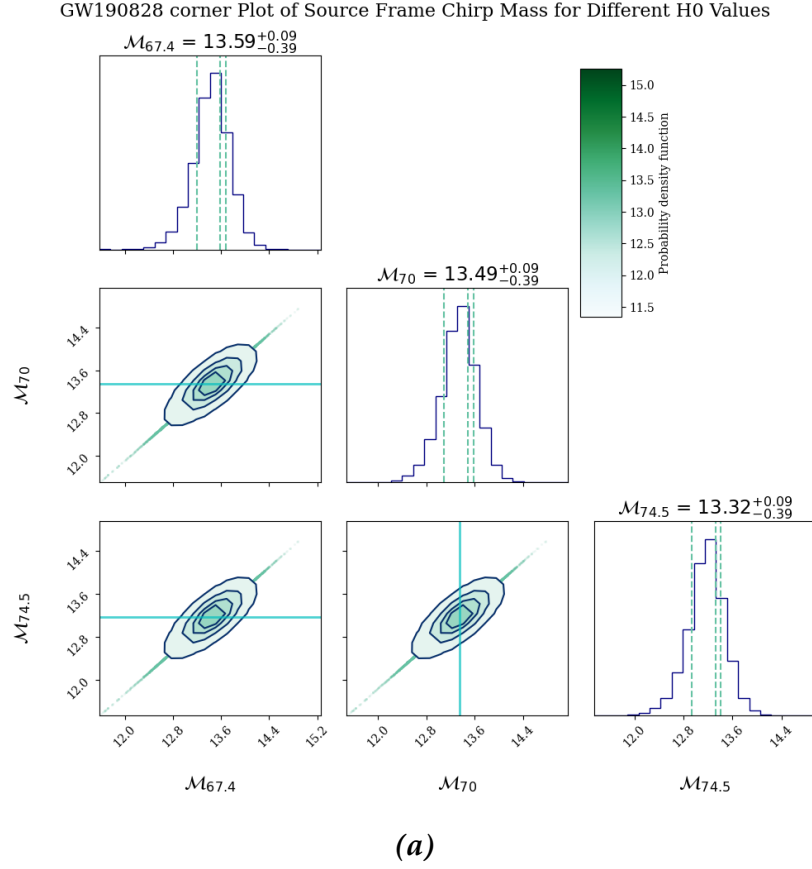**Figure 4.6:** *GW200224: (a) Corner plot for the chirp mass, and (b) contour plot showing the chirp mass as a function of the redshift.*

GW200311_115853 corner Plot of Source Frame Chirp Mass for Different H0 Values
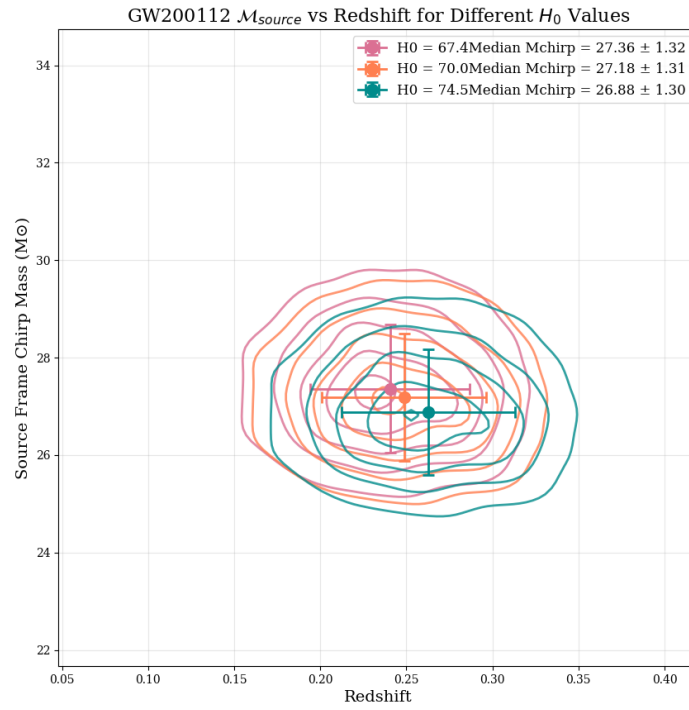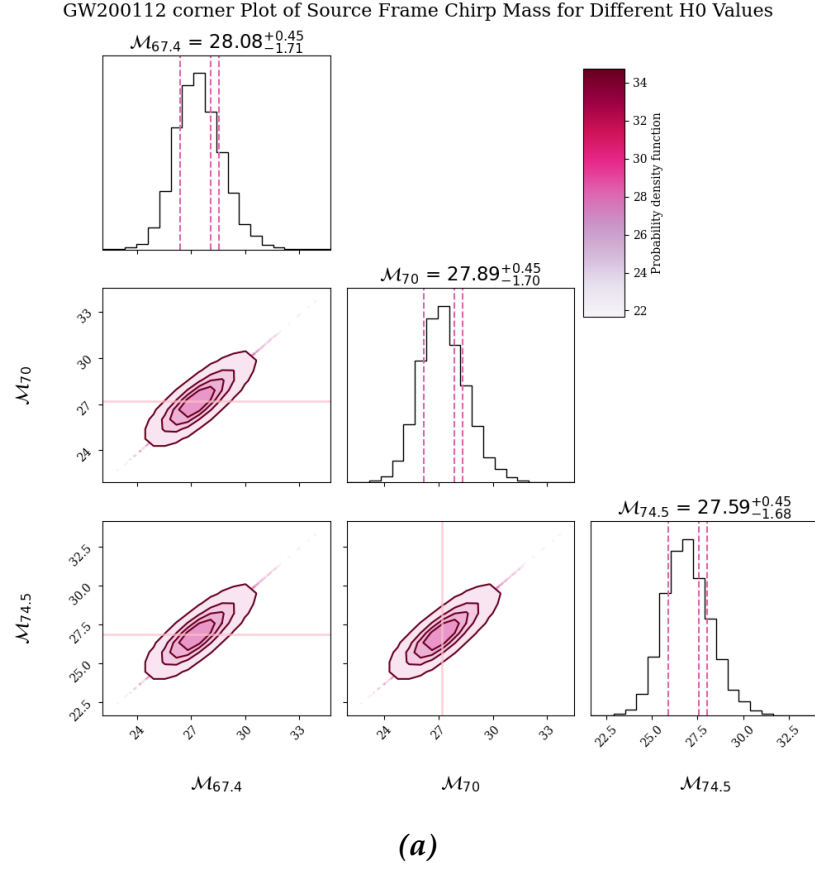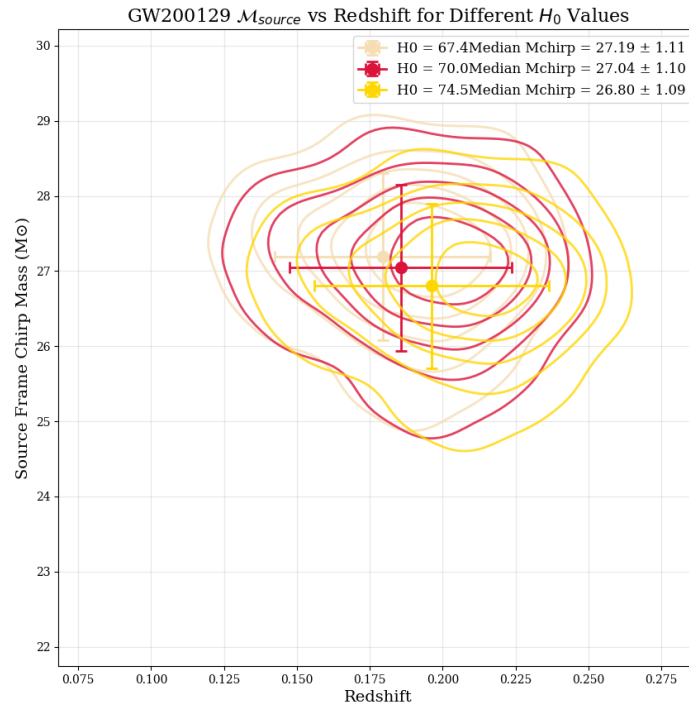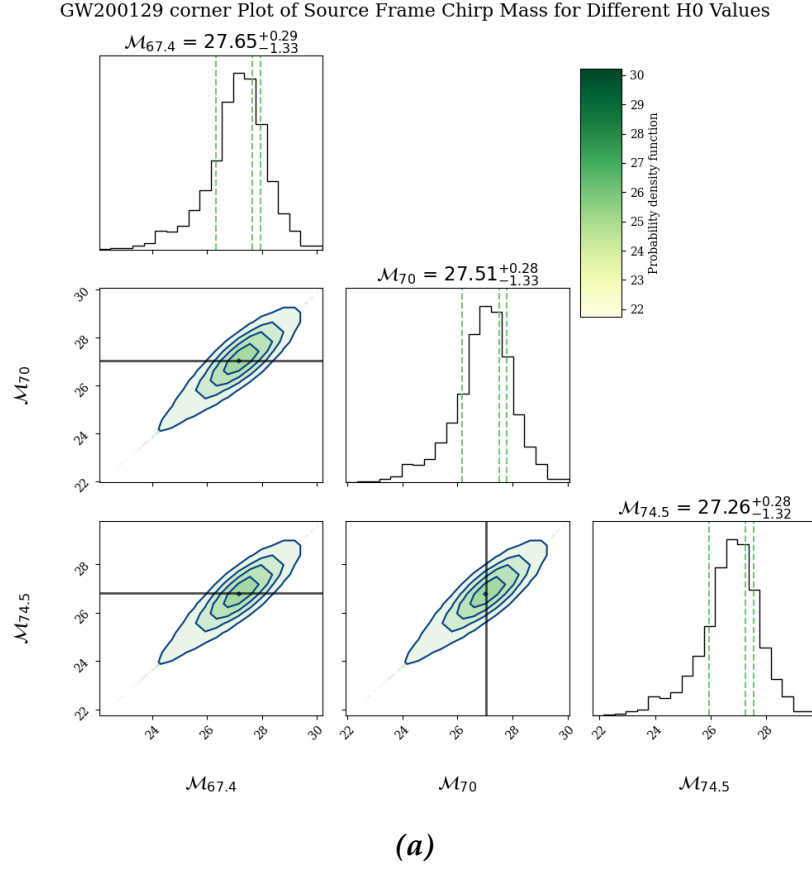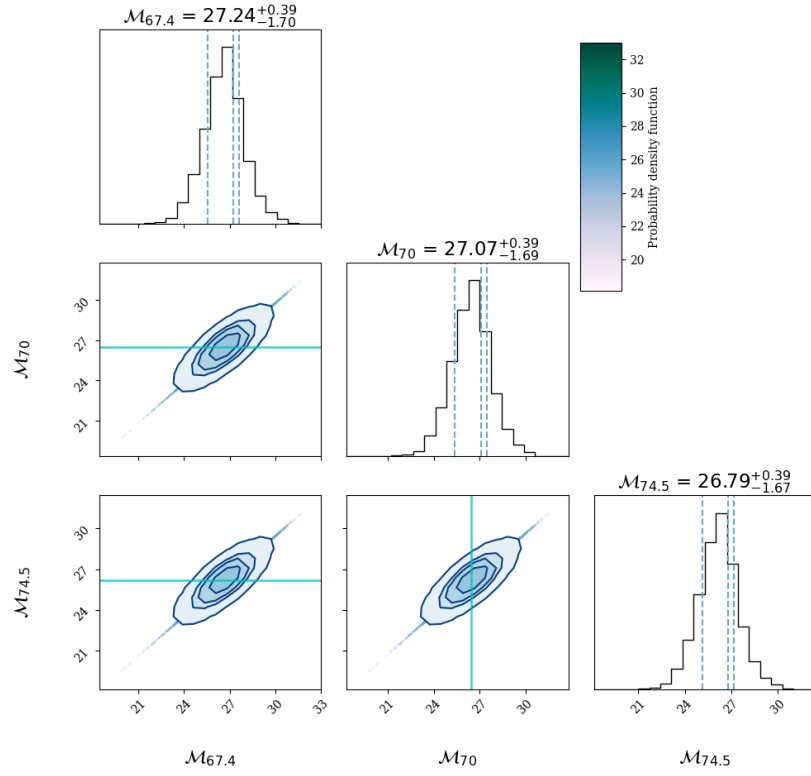

(a)
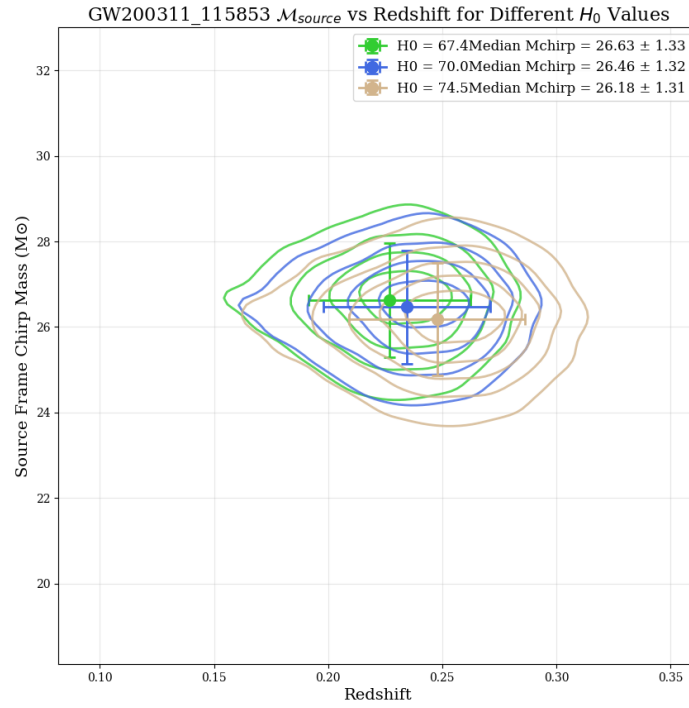
(b)

Figure 4.7: *GW200311 : (a) Corner plot for the chirp mass, and (b) contour plot showing the chirp mass as a function of the redshift.*

Chapter 5

DISCUSSION

5.1 Results analysis

5.1.1 Discussion on the redshift

The larger deviation in the redshift values corresponds to the highest redshift events ($GW200224\_222234$, $GW190828\_063405$). These were expected from the equation 2.22, where objects occurring at higher redshifts are more likely to be affected by cosmology and the expansion rate of the universe. See figure 5.1 and 5.2 for more insights.
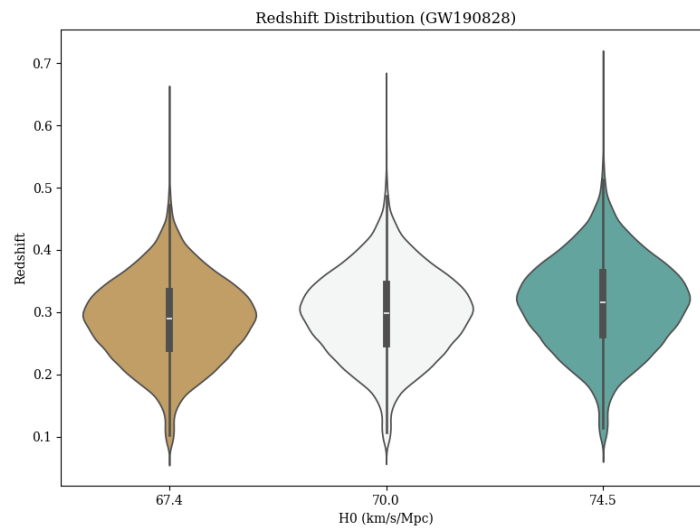
Figure 5.1: $GW190828\_063405$ *kernel density function distribution as violin plot, where the width indicates the "highest frequency" of the redshift data*
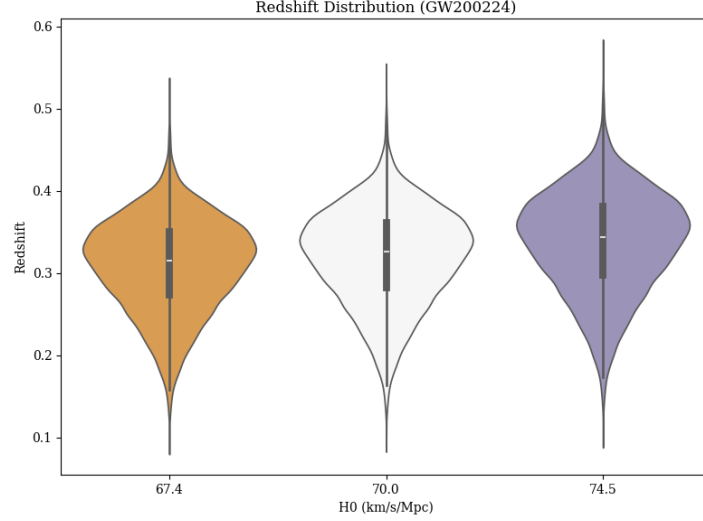
Figure 5.2: $GW200224\_222234$ *kernel density function distribution as violin plot.*

The redshift values for the remaining events were nearly equal, with minimal deviation, indicating that the redshift is low and that the cosmological effects are not significant.

5.1.2 Discussion on the chirp mass

The chirp mass values are systematically changing by altering H_0. Values of H_0 at high discrepancies (74.5) lead to the lowest chirp mass estimations. Nevertheless, chirp mass values obtained using a highly reliable measurement method (CMB 68.4) and other enhanced analyses (standard siren 70) are approximately equal. A T-test is conducted to assess the difference, and it was found to be a relatively significant difference:

- H0=67.4 vs H0=70.0: t-statistic = 6.8040, p-value = 0.0005

- H0=70.0 vs H0=74.5: t-statistic = 6.8877, p-value = 0.0005

- H0=67.4 vs H0=74.5: t-statistic = 6.8564, p-value = 0.0005

However, Cohen's d effect size ($H0 = 67.4 vs H0 = 74.5$) : 0.0696 indicates that the magnitude of the effect is small. Hence, **we cannot draw a conclusion about the chirp mass based on the current statistical results**.
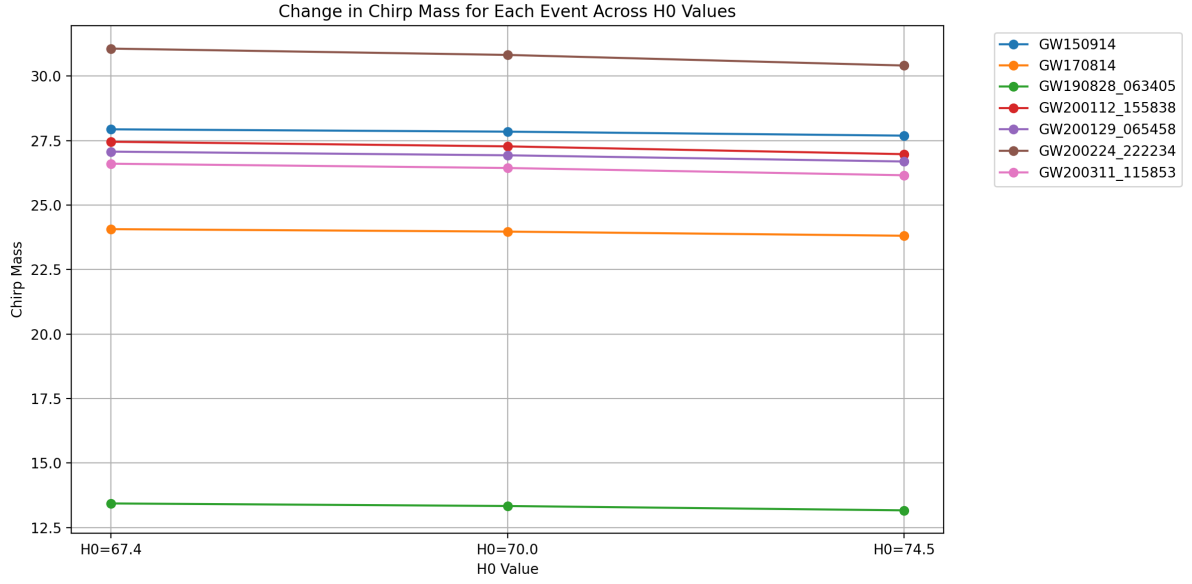
Figure 5.3: *Assessing the difference between each H_0 corresponding chirp mass values*

5.1.3 Fitting the Data

The strain amplitude is inversely proportional to the luminosity distance, defined by a factor of the chirp mass(Alfradique et al., 2024). Hence, an expected correlation exists between parameters related to the strain, such as the **radiated energy** and the chirp mass. By fitting all the values for each parameter, a moderate correlation was found $R \approx 0.5$ for all the values, with the best fit for the measurements of (CMB≈ 68.4). This can be interpreted as a "statistical bias" in the "re-weighted" values used close to the value $H_0 = 67.7$ depending on the Planck 2018 results.(R. Abbott, Abbott, et al., 2023). Furthermore, the high p-values indicate that the correlation is not significant and thus no such correlation is found.
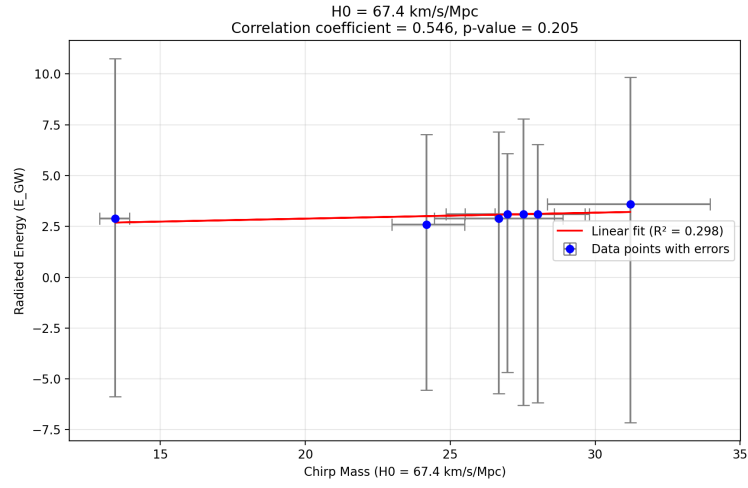
(a)
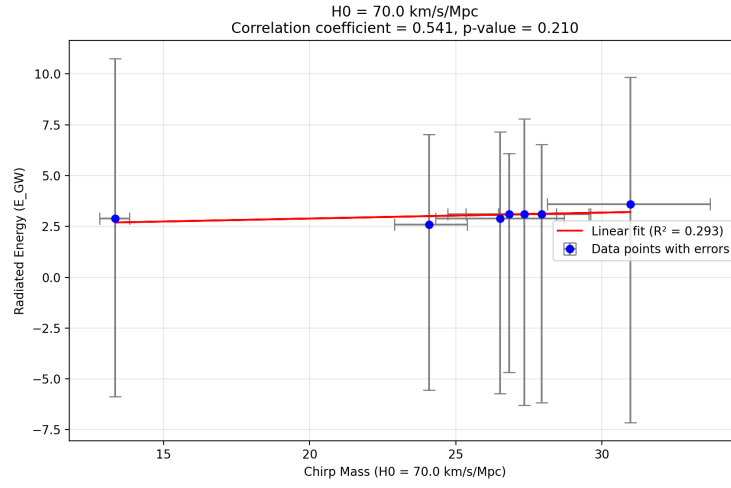
(b)
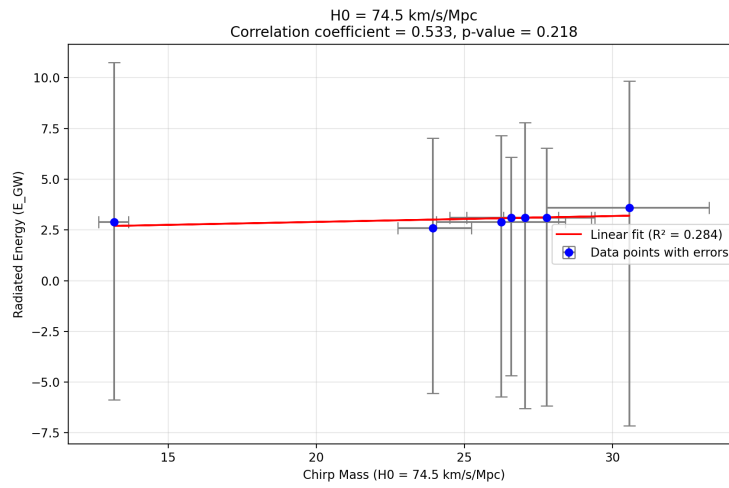
(c)

Figure 5.4: *The best linear fit of the three H_0 chirp mass values with the corresponding radiated energy of the GW signal*

5.2   limitation

The impact of Hubble tension on the current GWs observations was not statistically significant, as observed by the above analysis. However, the provided analysis needs many enhancements and further investigations. We can highlight the main limitations of the study as:

- The chirp mass results of a confident H_0 measurement method, the cosmic microwave background, showed close values to those from numerical relativity, calculated considering the general relativity correlation, implying that our framework is valid for such systems.

- The study analysis focused on low-redshift events z and did not include the effects of high-redshift mergers. So far, detected gravitational wave CBCs are confined to a limited redshift range of $0.1 \leq z \leq 1.2$.

- The results are subject to the inevitable uncertainty of the luminosity distance D_L values inferred from the GW signals, which lie within the degeneracy of the orbital inclination during the Inspiral phase (Mastrogiovanni et al., 2024), where the data size of this study is small and error analysis was not considered or addressed, further improvements are needed.

- It is important to note that the posterior data used in this study were reweighed, and a previous prior was assumed to have a uniform merging rate (B. P. Abbott et al., 2019),(R. Abbott, Abbott, Abraham, Acernese, Ackley, Adams, Adams, Adhikari, et al., 2021),(R. Abbott, Abbott, et al., 2023) which introduces a "statistical bias" in our results.

Inferring the luminosity distances and considering different waveform models is beyond the scope of this study, and we leave it to future work and further investigations. Such an error can be reduced by further EM counterpart, which was done by enhancing the "Bright serin" measurements with the case of (B. P. Abbott et al., 2017). However, most of the detected GW events are not associated with EM counterparts; we are

left with a less confident "Dark Serin" method to infer the cosmology parameters with the current state of the ground-based observatories!

5.2.1 Future work

So far, we have focused on only a small number of data points and equal-mass black hole systems and did not include other astrophysical scenarios. We might consider neutron star events, such as GW170817, for more insights. The next step will be to consider gravitational wave population events; future hypotheses can be well addressed. Additional parameters might be considered to have the potential to study the effects of cosmology, such as matter density Ω_{m}.

5.3 Conclusion

The chirp mass values in the source frame, along with the statistical analysis of the seven events of equal mass binaries, were computed and interpreted using Python. The results analysis showed an agreement with the The methodology we proposed enabled the analysis of the effect of H_0 on the inferred chirp mass across different Hubble parameter assumptions, offering insights into the impact of cosmological parameters on gravitational wave parameter inference.

The degeneracy between estimating the redshift and the chirp mass of the source was observed in this study, where most of the gravitational waves lack electromagnetic observations. It was observed that gravitational waves(GWs) are not sensitive enough to pin down the Hubble constant at the current stage of observations.

Future gravitational wave observatories promise to provide much-enhanced sky localization (The next Einstein Telescope generation in the next few years) and, therefore, more electromagnetic counterparts that will offer improved cosmological inference using gravitational waves (GWs) with even higher redshifts $z \approx 10$ for black hole binary systems(BBHs) and $z \approx 3$ for neutron star binaries (NSBs)(Mastrogiovanni et al., 2024), serving as a more robust tool to probe cosmology and pin down H_0 parameters.

BIBLIOGRAPHY

Abbott, B. P. (2017). Multi-messenger observations of a binary neutron star merger.

Abbott, B. P., Abbott, R., Abbott, T., Abernathy, M., Acernese, F., Ackley, K., Adams, C., Adams, T., Addesso, P., Adhikari, R., et al. (2016). Gw150914: The advanced ligo detectors in the era of first discoveries. *Physical review letters*, *116*(13), 131103.

Abbott, B. P., Abbott, R., Abbott, T., Acernese, F., Ackley, K., Adams, C., Adams, T., Addesso, P., Adhikari, R. X., Adya, V. B., et al. (2017). Gw170817: Observation of gravitational waves from a binary neutron star inspiral. *Physical review letters*, *119*(16), 161101.

Abbott, B. P., Abbott, R., Abbott, T., Abraham, S., Acernese, F., Ackley, K., Adams, C., Adhikari, R., Adya, V., Affeldt, C., et al. (2019). Gwtc-1: A gravitational-wave transient catalog of compact binary mergers observed by ligo and virgo during the first and second observing runs. *Physical Review X*, *9*(3), 031040.

Abbott, B., Abbott, R., Abbott, T., Abraham, S., Acernese, F., Ackley, K., Adams, C., Adhikari, R. X., Adya, V., Affeldt, C., et al. (2019). Tests of general relativity with the binary black hole signals from the ligo-virgo catalog gwtc-1. *Physical Review D*, *100*(10), 104036.

Abbott, R., Abe, H., Acernese, F., Ackley, K., Adhicary, S., Adhikari, N., Adhikari, R., Adkins, V., Adya, V., Affeldt, C., et al. (2023). Open data from the third observing run of ligo, virgo, kagra and geo. *arXiv preprint arXiv:2302.03676*.

Abbott, R., Abe, H., Acernese, F., Ackley, K., Adhikari, N., Adhikari, R., Adkins, V., Adya, V., Affeldt, C., Agarwal, D., et al. (2021). Tests of general relativity with gwtc-3. *arXiv preprint arXiv:2112.06861*.

Abbott, R., Abbott, T., Abraham, S., Acernese, F., Ackley, K., Adams, A., Adams, C., Adhikari, R., Adya, V., Affeldt, C., et al. (2021). Gwtc-2: Compact binary coalescences observed by ligo and virgo during the first half of the third observing run. *Physical Review X*, *11*(2), 021053.

Abbott, R., Abbott, T., Acernese, F., Ackley, K., Adams, C., Adhikari, N., Adhikari, R., Adya, V., Affeldt, C., Agarwal, D., et al. (2023). Gwtc-3: Compact binary coalescences observed by ligo and virgo during the second part of the third observing run. *Physical Review X*, *13*(4), 041039.

Abbott, R., Abbott, T., Abraham, S., Acernese, F., Ackley, K., Adams, A., Adams, C., Adhikari, R. X., Adya, V., Affeldt, C., et al. (2021). Tests of general relativity with binary black holes from the second ligo-virgo gravitational-wave transient catalog. *Physical review D*, *103*(12), 122002.

Alfradique, V., Bom, C. R., Palmese, A., Teixeira, G., Santana-Silva, L., Drlica-Wagner, A., Riley, A., Martínez-Vázquez, C. E., Sand, D., Stringfellow, G. S., et al. (2024). A dark siren measurement of the hubble constant using gravitational wave events from the first three ligo/virgo observing runs and delve. *Monthly Notices of the Royal Astronomical Society*, *528*(2), 3249–3259.

Bailes, M., Berger, B. K., Brady, P., Branchesi, M., Danzmann, K., Evans, M., Holley-Bockelmann, K., Iyer, B., Kajita, T., Katsanevas, S., et al. (2021). Gravitational-wave physics and astronomy in the 2020s and 2030s. *Nature Reviews Physics*, *3*(5), 344–366.

Chattopadhyay, D., Al-Shammari, S., Antonini, F., Fairhurst, S., Miles, B., & Raymond, V. (2024). The impact of astrophysical priors on parameter inference for gw230529. *Monthly Notices of the Royal Astronomical Society: Letters*, slae099.

Chen, A., Gray, R., & Baker, T. (2024). Testing the nature of gravitational wave propagation using dark sirens and galaxy catalogues. *Journal of Cosmology and Astroparticle Physics*, *2024*(02), 035.

Chen, Z.-C., & Liu, L. (2024). Constraining the nonstandard propagating gravitational waves in the cosmological background with gwtc-3. *arXiv preprint arXiv:2405.10031.*

Choudhary, S. (2024). Compact binary coalescence searches: Gravitational wave open data workshop.

DeWitt, C. M., & Rickles, D. (2011). *The role of gravitation in physics: Report from the 1957 chapel hill conference.* Edition Open Access.

Einstein, A. (1915). On the general theory of relativity (addendum). *SITZUNGSBERICHTE DER KONIGLICH PREUSSISCHEN AKADEMIE DER WISSENSCHAFTEN, 799.*

Gair, J. (2019). Making sense of data: Introduction to statistics for gravitational wave astronomy. https://www.aei.mpg.de

Husa, S. (2009). Michele maggiore: Gravitational waves. volume 1: Theory and experiments. *General Relativity and Gravitation, 41*(7), 1667–1669.

Maggiore, M. (2018). *Gravitational waves: Volume 2: Astrophysics and cosmology.* Oxford University Press.

Maione, F., De Pietri, R., Feo, A., & Löffler, F. (2017). Spectral analysis of gravitational waves from binary neutron star merger remnants. *Physical Review D, 96*(6), 063011.

Mastrogiovanni, S., Karathanasis, C., Gair, J., Ashton, G., Rinaldi, S., Huang, H.-Y., & Dálya, G. (2024). Cosmology with gravitational waves: A review. *Annalen der Physik, 536*(2), 2200180.

Ohme, F. (2011). Analytical meets numerical relativity: Status of complete gravitational waveform models for binary black holes. *Classical and Quantum Gravity, 29.* https://api.semanticscholar.org/CorpusID:118658849

Scientific, L., & Collaborations, V. (2017). The basic physics of the binary black hole merger gw150914. *Ann. Phys*, *529*(1-2), 1600209.

Taylor, J. H., Fowler, L. A., & McCulloch, P. M. (1979). Measurements of general relativistic effects in the binary pulsar psr1913+ 16. *Nature*, *277*(5696), 437–440.

Verde, L., Schöneberg, N., & Gil-Marín, H. (2023). A tale of many h 0. *Annual Review of Astronomy and Astrophysics*, *62*.

Weber, J. (1960). Detection and generation of gravitational waves. *Physical Review*, *117*(1), 306.

Weber, J. (1971). The detection of gravitational waves. *Scientific American*, *224*(5), 22–29.

Appendix A

APPENDIX A

A.1 A Section

```
GW170814 ='/content/drive/MyDrive/ 1_datasets/GW170814_103043_cosmo.h5'
posterior2 = h5py.File(GW170814, 'r')
samples2=pd.DataFrame.from_records(np.array(posterior2['CO1:Mixed']['
    posterior_samples']))
```

Code Listing A.1: *Accesing the posterior data (for a single event GW170814) and choosing the waveform model*

```
#Data proccesing
luminosity_distance = posterior2['CO1:Mixed']['posterior_samples']['
    luminosity_distance']
sample_size = len(luminosity_distance)  # Use the full dataset
# To Access luminosity distance values from posterior_samples
def process_cosmological_data(luminosity_distance, h0_values,
    sample_size):
    results_data = []
    for h0 in h0_values:
        cosmo = FlatLambdaCDM(H0=h0, Om0=0.3)
        redshifts = [float(z_at_value(cosmo.luminosity_distance, d * u.
    Mpc).value)
                    for d in luminosity_distance[:sample_size]]
        for z in redshifts:
            results_data.append({
                'H0': h0,
                'redshift': z,
                'luminosity_distance': luminosity_distance[redshifts.
    index(z)]
            })
```

47

```
    return pd.DataFrame(results_data)


# Process the data
h0_values = [67.4, 70.0, 74.5]  #CMB, Standard Serin, Time lensing
    delay
df = process_cosmological_data(luminosity_distance, h0_values,
    sample_size)  #luminosity distance  from array to the function
```

Code Listing A.2: Estimating the redshift over loop of H0 parameters

```
#Storing the computed redshift values for different H0
redshift_h0_67 = df[df['H0'] == 67.4]['redshift'].values #calculated
redshift_h0_70 = df[df['H0'] == 70.0]['redshift'].values #calculated
redshift_h0_74 = df[df['H0'] == 74.5]['redshift'].values #calculated
redshift_litreture = posterior2['C01:Mixed']['posterior_samples']['
    redshift'] #from the published data
median_redshift_litreture = np.median(redshift_litreture)
std_redshift_litreture = np.std(redshift_litreture)
```

Code Listing A.3: Estimated redshift values

```
mchirp = ((samples2['mass_1'] * samples2['mass_2'])**(3./5))/\
         (samples2['mass_1'] + samples2['mass_2'])**(1./5)


# computing the chirp mass values at the three redshift values
mchirp_source_sample1A = mchirp / (1 + z_67_4)
mchirp_source_sample1B = mchirp / (1 + z_70_0)
mchirp_source_sample1C = mchirp / (1 + z_74_5)


# calculating the chirp mass from the public data
redshift_litreture = posterior2['C01:Mixed']['posterior_samples']['
    redshift']
numirical_relativity = posterior2['C01:Mixed']['posterior_samples']['
    chirp_mass']
numirical_relativity = numirical_relativity / (1 + redshift_litreture)
numirical_relativity = np.median(numirical_relativity)
std_numirical_relativity = np.std(numirical_relativity)
```

Code Listing A.4: The Python code calculating the detector frame chirp mass

48

```python
data = np.array([mchirp_source_samplelA, mchirp_source_samplelB,
    mchirp_source_samplelC]).T


# Calculate medians and standard deviations
median_mchirp_A = np.median(mchirp_source_samplelA)

median_mchirp_B = np.median(mchirp_source_samplelB)

median_mchirp_C = np.median(mchirp_source_samplelC)

std_mchirp_A = np.std(mchirp_source_samplelA)

std_mchirp_B = np.std(mchirp_source_samplelB)

std_mchirp_C = np.std(mchirp_source_samplelC)


# Set style parameters
plt.style.use('default')

plt.rcParams['axes.grid'] = False
# Styling the corner plots
cmap = plt.cm.Oranges

plt.rcParams['font.family'] = 'DejaVu Serif'

figure = corner.corner(data,
                       labels=[r"$\mathcal{M}_{67.4}$", r"$\mathcal{M}_
    {70}$",

                               r"$\mathcal{M}_{74.5}$"],

                       show_titles=True,

                       title_kwargs={"fontsize": 16.5},

                       label_kwargs={"fontsize": 16.5},

                       quantiles=[0.2, 0.7, 0.8],

                       title_fmt=".2f",

                       plot_datapoints=True,

                       plot_density=True,

                       fill_contours=True,

                       color=cmap(0.5),

                       contour_kwargs={'colors': plt.cm.BuPu(
                           np.linspace(8, 6, 2))},

                       smooth=1.0,

                       labelsize=16,

                       levels=[0.1, 0.3, 0.5, 0.7, 0.9],

                       hist_kwargs={'color': 'sienna'}
                       )


# Add colorbar
```

49

```python
norm = Normalize(vmin=min(data.flatten()), vmax=max(data.flatten()))
sm = ScalarMappable(cmap=cmap, norm=norm)
sm.set_array([])


# Add the colorbar to the right side of the plot
cbar_ax = figure.add_axes([0.7, 0.6, 0.05, 0.3])  # [left, bottom,
    width, height]
cbar = plt.colorbar(sm, cax=cbar_ax, label='Probability density
    function')


# Access individual subplot
axes = figure.axes
# Figure itle
figure.suptitle("GW170814 corner Plot of Source Frame Chirp Mass for
    Different H0 Values", fontsize=16)
# Adding median lines
axes[3].axhline(median_mchirp_B, color='peru', alpha=0.7, linewidth=2)
axes[6].axhline(median_mchirp_C, color='peru', alpha=0.7, linewidth=2)
axes[7].axvline(median_mchirp_B, color='peru', alpha=0.7, linewidth=2)
# Adjust figure dim
figure.set_size_inches(10,10)
plt.tight_layout()
from google.colab import files
plt.savefig('corner2b_plot.png')
files.download('corner2b_plot.png')
plt.show
```

Code Listing A.5: Creating corner plot for the chirp mass values

```python
    import matplotlib.pyplot as plt
from scipy import stats
#Creating the plot
plt.figure(figsize=(10, 10))


# Ploting contours for each H0 value
colors = ['mediumseagreen', 'crimson', 'cornflowerblue']


labels = ['H0 = 67.4', 'H0 = 70.0', 'H0 = 74.5']
plt.rcParams['font.family'] = 'DejaVu Serif'
```

```python
for i, (z, m, median_m, std_m, color, label) in enumerate(zip(
    [redshift_h0_67, redshift_h0_70, redshift_h0_74],
    [mchirp_source_sample1A, mchirp_source_sample1B,
   mchirp_source_sample1C],
    [median_mchirp_A, median_mchirp_B, median_mchirp_C],  #Previously
   defined
    [std_mchirp_A, std_mchirp_B, std_mchirp_C],
    colors, labels)):

    # This command to ensure z and m have the same length
    z_repeated = np.repeat(z, len(m) // len(z) + 1)[:len(m)]

    # Calculating the kernel density estimate
    xmin, xmax = z_repeated.min(), z_repeated.max()
    ymin, ymax = m.min(), m.max()
    xx, yy = np.mgrid[xmin:xmax:100j, ymin:ymax:100j]
    positions = np.vstack([xx.ravel(), yy.ravel()])
    values = np.vstack([z_repeated, m])  # Use z_repeated here
    kernel = stats.gaussian_kde(values)
    f = np.reshape(kernel(positions).T, xx.shape)

    # Ploting contours only (no filled contours)
    plt.contour(xx, yy, f, levels=5, colors=color, alpha=0.8,
   linewidths=2)

    # Ploting the median and error bars
    plt.errorbar(np.median(z), median_m,
                xerr=np.std(z), yerr=std_m,
                color=color, marker='o', markersize=10,
                capsize=5, capthick=2, linewidth=2,
                label=f'{label}\
Median Mchirp = {median_m:.2f}    {std_m:.2f}')

plt.xlabel('Redshift', fontsize=14)
plt.ylabel('Source Frame Chirp Mass ( M  )', fontsize=14)
plt.title('GW170814 $\mathcal{M}_{source}$ vs Redshift for Different
   $H_0$ Values', fontsize=16)
plt.legend(fontsize=12, bbox_to_anchor=(1, 1), loc='upper right')
plt.grid(True, alpha=0.3)
```

51

```python
from google.colab import files
plt.savefig("plot2c.png")
files.download("plot2c.png")
plt.show()


# Set white background
plt.gca().set_facecolor('white')
plt.gcf().set_facecolor('white')
# Print the statistical summary
print(f"H0 = 67.4: Mchirp = {median_mchirp_A:.2f}")
print(f"H0 = 70.0: Mchirp = {median_mchirp_B:.2f}")
print(f"H0 = 74.5: Mchirp = {median_mchirp_C:.2f}")
```

Code Listing A.6: *Countor plot for the chirp mass and redshift values*